



January 2021

Investigation Of Cats Aerosol Products And Application Toward Global Diurnal Variation Of Aerosols

Logan Lee

[How does access to this work benefit you? Let us know!](#)

Follow this and additional works at: <https://commons.und.edu/theses>

Recommended Citation

Lee, Logan, "Investigation Of Cats Aerosol Products And Application Toward Global Diurnal Variation Of Aerosols" (2021). *Theses and Dissertations*. 4172.

<https://commons.und.edu/theses/4172>

This Thesis is brought to you for free and open access by the Theses, Dissertations, and Senior Projects at UND Scholarly Commons. It has been accepted for inclusion in Theses and Dissertations by an authorized administrator of UND Scholarly Commons. For more information, please contact und.common@library.und.edu.

INVESTIGATION OF CATS AEROSOL PRODUCTS AND APPLICATION
TOWARD GLOBAL DIURNAL VARIATION OF AEROSOLS

by

Logan Patrick Lee
Bachelor of Science, University of North Dakota, 2015

A Thesis

Submitted to the Graduate Faculty

of the

University of North Dakota

in partial fulfillment of the requirements

for the degree of

Master of Science

Grand Forks, North Dakota

December
2021

Copyright 2021 Logan Lee

Name: Logan Lee
Degree: Master of Science


This document, submitted in partial fulfillment of the requirements for the degree from the University of North Dakota, has been read by the Faculty Advisory Committee under whom the work has been done and is hereby approved.

DocuSigned by:


2707AED4619A416...
Jianglong Zhang

DocuSigned by:

A84ADF8F371R443...
Jeffrey Reid

DocuSigned by:

813D3F7026A9558...
Aaron Kennedy

This document is being submitted by the appointed advisory committee as having met all the requirements of the School of Graduate Studies at the University of North Dakota and is hereby approved.

DocuSigned by:

2E0AF088C733403...
Chris Nelson
Dean of the School of Graduate Studies
11/29/2021

Date

PERMISSION

Title Investigation of CATS Aerosol Products and Application Toward
 Global Diurnal Variation of Aerosols

Department Atmospheric Sciences

Degree Master of Science

In presenting this thesis in partial fulfillment of the requirements for a graduate degree from the University of North Dakota, I agree that the library of this University shall make it freely available for inspection. I further agree that permission for extensive copying for scholarly purposes may be granted by the professor who supervised my thesis work or, in his absence, by the Chairperson of the department or the dean of the School of Graduate Studies. It is understood that any copying or publication or other use of this thesis or part thereof for financial gain shall not be allowed without my written permission. It is also understood that due recognition shall be given to me and to the University of North Dakota in any scholarly use which may be made of any material in my thesis.

Logan Lee
September 26, 2021

TABLE OF CONTENTS

LIST OF FIGURES.....	vi
LIST OF TABLES.....	viii
ACKNOWLEDGEMENTS.....	ix
ABSTRACT.....	x
CHAPTER	
1. INTRODUCTION.....	1
2. DATA AND METHODOLOGY.....	6
2.1. CATS.....	6
2.2. AERONET.....	9
2.3. MODIS Collection 6.1 Dark Target Product.....	10
2.4. CALIOP.....	11
2.5. Collocation Methodology.....	13
2.5.1. AERONET.....	13
2.5.2. MODIS.....	13
2.5.3. CALIOP.....	14
3. RESULTS AND DISCUSSION.....	16
3.1. CATS-AERONET.....	16
3.2. CATS-MODIS.....	17
3.3. CATS-CALIOP AOD.....	18
3.4. CATS-CALIOP Vertical Extinction Profiles.....	25
3.5. Application: Diurnal Cycle of AODs and Aerosol Vertical Distributions....	29
3.5.1. Seasonal and Diurnal Variation of AOD.....	29
3.5.2. Diurnal Variations of Aerosol Extinction on a Global Scale (both at UTC and local time).....	34
3.5.3. Diurnal Variations of Aerosol Extinction on a Regional Scale (at local time).....	37
3.5.4. Comparison to Previous Studies.....	42
3.5.5. Some Potential Mechanisms for Diurnal Aerosol Variability....	43
4. CONCLUSIONS.....	48
APPENDIX A.....	52
REFERENCES.....	53

LIST OF FIGURES

Figure	Page
1.	Collocated AERONET 1020 nm AOT vs. CATS 1064 nm AOD a) without CATS QA applied, and b) with CATS QA applied.....17
2.	Collocated MODIS C6.1 a) Terra and b) Aqua interpolated 1064 nm AOD vs. CATS 1064 nm AOD with CATS QA applied.18
3.	Collocated CALIOP 1064 nm AOD vs. CATS 1064 nm AOD with CATS QA applied for a) both day and night, b) nighttime over-land, c) nighttime over-water, d) daytime over-land, e) daytime over-water.20
4.	CATS 1064 nm AOD a) as a function of local time for the globe, and b) as a function of local time for areas south of -25 degrees. The difference between CATS 1064 nm AOD and AERONET 1020 nm AOD as a function of local time is shown in c). The mean is represented by the blue line, while the median is the green line.24
5.	CATS and CALIOP vertical profiles of 1064 nm extinction for a) all profiles, b) daytime only, c) nighttime only, d) over-water, and e) over land. f) shows the difference between CATS and CALIOP mean 1064 nm extinction for all collocated profiles (5a) as a function of height. Mean AOD values are as follows: for CATS: a) 0.094 , b) 0.091 , c) 0.098, d) 0.088, e) 0.119, and for CALIOP: a) 0.093, b) 0.092, c) 0.093, d) 0.084, e) 0.127.28
6.	Mean AOD (1064 nm) by season for a) DJFMAM CATS, b) JJASON CATS, c) DJFMAM CALIOP, d) JJASON CALIOP, e) DJFMAM MODIS Aqua, and f) JJASON MODIS Aqua. Red boxes indicate locations of regional vertical distributions in Figures 12 and 13.31
7.	Mean CATS AOD (1064 nm) by season for a) DJFMAM below 1 km AGL, b) JJASON below 1 km AGL, c) DJFMAM 1-2 km AGL, d) JJASON 1-2 km AGL, e) DJFMAM above 2 km AGL, and f) JJASON above 2 km AGL.32
8.	Seasonal Mean AOD (1064 nm) binned by every 6-hours for a) DJFMAM 0 UTC, b) JJASON 0 UTC, c) DJFMAM 6 UTC, d) JJASON 6 UTC, e) DJFMAM 12 UTC, f) JJASON 12 UTC, g) DJFMAM 18 UTC, and h) JJASON 18 UTC. .33
9.	Maximum minus minimum mean seasonal AOD (1064 nm) for a) DJFMAM, and b) JJASON.34

10.	Global mean 6-hourly vertical profiles of CATS 1064 nm extinction for a) DJFMAM all profiles, b) DJFMAM water profiles, c) DJFMAM not-water profiles, d) JJASON all profiles, e) JJASON water profiles, f) JJASON not-water profiles. Mean AODs are as follows: a) 0.084, b) 0.078, c) 0.098, d) 0.089, e) 0.082, and f) 0.102.	36
11.	Global mean 6-hourly local time (0:00 am, 6:00 am, 12:00 pm and 6:00 pm) vertical profiles of CATS 1064 nm extinction for a) DJFMAM all profiles, b) DJFMAM water profiles, c) DJFMAM not-water profiles, d) JJASON all profiles, e) JJASON water.	37
12.	DJFMAM 6-hourly average (local time; 0:00 am, 6:00 am, 12:00 pm and 6:00 pm) vertical profiles of CATS 1064 nm for locations shown in Figure 6a; a) Africa-North, b) Middle East, c) India, and d) Northeast China.	40
13.	JJASON 6-hourly average (local time; 0:00 am, 6:00 am, 12:00 pm and 6:00 pm) vertical profiles of CATS 1064 nm for locations shown in Figure 6b; a) Africa-North, b) Africa-South, c) Middle East, d) India, and e) Northeast China.	41
A1.	Collocated AERONET 1020 nm AOT vs. CATS 1064 nm AOD a) without CATS QA applied, and b) with CATS QA applied. CATS V2-01 aerosol products were used in constructing this plot.	52

LIST OF TABLES

Table	Page
1. Descriptive statistical properties between collocated CATS and AERONET, CALIOP and Aqua MODIS AOD retrievals. Here STDDEV indicates standard deviation of AOD and R-value represents the correlation coefficient.	20
2. Sensitivity study of descriptive statistical properties between collocated CATS and AERONET, CALIOP and Aqua MODIS AOD retrievals by varying spatial and temporal collocation windows. Here STDDEV indicates standard deviation of AOD and R-value represents the correlation coefficient.	21
3. CALIOP and CATS mean AODs / AOD standard deviations for regions as highlighted in Figure 6 and globally between +/- 52° latitude.	31
4. Geographic ranges, height above ground level of maximum extinction, diurnal extinction range at height of maximum extinction, and time (local) of peak extinction for the boxed red regions in Figure 6 and vertical profiles shown in Figures 12 and 13.	41

ACKNOWLEDGEMENTS

I would like to express my deep gratitude to my advisor, Dr. Jianglong Zhang, for his continual support, patience, and guidance through this process. I would also like to thank my committee members, Dr. Jeffrey Reid and Dr. Aaron Kennedy, for their guidance, support, and flexibility while completing this thesis. I am also grateful to Dr. John Yorks for providing guidance regarding the CATS data during this project.

Thank you to my parents and grandparents as well, who provided unwavering support for my studies over the years.

Lastly, I would like to thank my wonderful office-mates and the rest of the graduate students at UND for their support and friendship throughout my graduate career.

I would like to acknowledge the support of ONR grant (N00014-16-1-2040) and NASA grant (NNX17AG52G) for this study, and the support of NASA NESSF fellowship grant (NNX16A066H). I would also like to thank the NASA AERONET team for the AERONET data used in this study.

To my late grandpa Chuck,
whose faith in me was instrumental in completing this thesis.

Abstract

A comparison of 1064 nm aerosol optical depth (AOD) from the Cloud-Aerosol Transport System (CATS) with collocated Aerosol Robotic Network (AERONET), Aqua and Terra Moderate Imaging Spectroradiometer (MODIS) Dark Target, and Cloud-Aerosol Lidar with Orthogonal Polarization (CALIOP) AOD for the period of Mar. 2015-Oct. 2017 is presented in this study. In addition, vertical profiles of aerosol extinction from CATS and CALIOP are also compared for the same period. Upon quality assurance checks of CATS data, reasonable agreement is found between aerosol data from CATS and other sensors. Using quality assured CATS aerosol data, for the first time, variations in AODs and aerosol extinction profiles are evaluated at 00, 06, 12, and 18 UTC (and/or 0:00 am, 6:00 am, 12:00 pm and 6:00 pm local solar times) on both regional and global scales. This study suggests that marginal variations are found in AOD from a global mean perspective, with the minimum aerosol extinction values found at 6:00 pm (local time) near the surface layer for global oceans, for both the June-November and December-May seasons. Over land, below 500m, the daily minimum and maximum aerosol extinction values are found at 12:00pm and 00:00/06:00 am (local time), respectively. Strong diurnal variations are also found over Africa-North and India for the December-May season, and over Africa-North, Africa-South, Middle East, and India for the June-November season.

Chapter 1

Introduction

Small suspended particles in the air are known as atmospheric aerosols (Wallace and Hobbs 2006). Atmospheric aerosols come from a variety of both man-made and natural sources, and include smoke, sea salt, dust, and pollen (Wallace and Hobbs 2006). It has long been recognized that aerosols can impact climate through reflection and absorption of solar and terrestrial radiation (Ramanathan et. al 2001). In addition, aerosols have been shown to reduce downward surface shortwave flux and thus impact daytime surface temperatures, as well as other weather-related properties such as wind and planetary boundary layer height (Zhang et al. 2016; Carson-Marquis et al. 2021). Aerosols also impact the water cycle through their roles as cloud condensation nuclei (Hartmann 2016), contribute to air pollution in many areas across the globe (Wallace and Hobbs 2006), and reduce visibility in arid regions (Warner 2004). Because of the multitude of aerosol-related impacts, several methods have been devised to measure and quantify aerosol concentrations in the atmosphere from both the ground and space (satellites).

Ground-based methods can involve either in situ observations of aerosols in the air, or remote sensing methods. In situ observations involve direct contact between instruments and the aerosols. Alternatively, remote sensing methods utilize electromagnetic radiation to measure properties of aerosols from a distance. One such set of ground-based remote sensors is known as the AErosol RObotic NETwork, or AERONET (Holben et al. 1998). AERONET sun photometers provide point-based daytime sampling with high temporal frequency, but until recently with the development of a lunar photometry mode, have been limited to daylight hours. Ground-based observations are often used as the ground truth for

satellite-based applications, yet the spatial coverage of ground-based instruments is limited due to the cost of deploying such instruments.

Space-borne sensors overcome some of the spatial limitations of ground-based sensors. However, these space-borne sensors have their own assumptions and uncertainties. Satellites can take advantage of either passive or active remote sensing to observe aerosol properties. Passive remote sensing is the measurement of electromagnetic radiation that is emitted or scattered by a target (Tedesco 2015). For conventional aerosol retrievals, the source of this radiation is the sun, which limits sampling to the daytime hours. Orbital characteristics can further limit the spatial and temporal characteristics of data sampling from satellites. Sun-synchronous, polar-orbiting satellites pass over locations on the ground at approximately the same local time every day, which provides only a small sampling of the full diurnal cycle. Geostationary satellite sensors such as the Advanced Himawari Imager (AHI) on Himawari 8 (Yoshida et al. 2018) and the Advanced Baseline Imager on GOES-16/17 (Aerosol Product Application Team of the AWG Aerosols/Air Quality/Atmospheric Chemistry Team 2012) remain over a fixed location on the earth, and are able to provide high temporal resolution measurements of aerosol particles over a given location. However, geostationary positioning means these satellites do not individually encompass the entire globe, and due to their design, do not have nighttime aerosol retrieval capability. These satellites also can have lower spatial resolution than polar orbiting instruments.

Active sensors emit a pulse of electromagnetic radiation and then measure the amount that is scattered back to the sensor by the target (Tedesco 2015). This provides the advantage of being capable of carrying out nighttime observations without reliance on

sunlight. However, the need to emit a pulse also limits the spatial extent compared to passive satellites. One particular type of active sensor is known as Light Detection And Ranging, or lidar. Lidar transmits pulses of laser light and then measures the time for the scattered laser energy to return to the sensor to calculate the distance between the sensor and the target. In addition, differences between the returned energy and the original pulse are used to characterize the properties of the medium and targets (Tedesco 2015). A unique advantage of lidar over other sensors is the ability to sample the vertical structure of aerosols in the atmosphere. The measurement of diurnal variations of aerosol properties resolved in the vertical is especially crucial for visibility and particulate matter forecasts. Indeed, the periods around sunrise and sunset show significant near surface variability that is difficult to detect with passive sensors. One such lidar, called the Cloud-Aerosol Lidar with Orthogonal Polarization (CALIOP), is widely used to study vertical distributions of aerosols. While lidar data from CALIOP provide early afternoon and morning observations, two temporal points and a 16-day repeat cycle are insufficient to evaluate the critical morning and evening hours where many key aerosol lifecycle processes take place.

Given the previously mentioned limitations, most satellite-based aerosol studies have been limited to daytime point observations or daily average points of view, yet we know that pollution (e.g., Zhao et al. 2009; Tiwari et al. 2013; Kaku et al. 2018), fires and smoke properties (e.g., Reid et al. 1999; Giglio et al. 2003; Hyer et al. 2013), and dust (e.g., Mbourou, et al. 1997; Fiedler et al. 2013; Heinold et al. 2013) can exhibit strong diurnal behavior. Some of the limiting factors in previous studies can be addressed by the Cloud-Aerosol Transport System (CATS) lidar that flew aboard the International Space Station (ISS) from 2015 to 2017 (McGill et al. 2015). The ISS's precessing orbit with a 51.6°

inclination is not sun-synchronous, which allows for 24-hour sampling of the tropics to the mid-latitudes, with the ability to observe aerosol and cloud vertical distributions at both day and night with high temporal resolution. For a given location within $\pm 51.6^\circ$ (latitude), after aggregating roughly 60 days of data, a near full diurnal cycle of aerosol and cloud properties can be obtained from CATS observations (Yorks et al. 2016). This provides a new opportunity for studying diurnal variations (day and night) in aerosol vertical distributions from space observations.

Use of CATS has its own challenges. Most importantly, CATS retrievals must cope with variable solar noise around the solar terminator where some of the strongest diurnal variability exists. Furthermore, CATS lost its 532 nm wavelength channel early in its deployment, leaving only a 1064 nm channel functioning. Aerosols and clouds possess different scattering characteristics at different wavelengths, which can be used to discriminate between them. The availability of only one wavelength limited the CATS cloud-aerosol discrimination algorithm, which can cause a loss of accuracy compared to CALIOP which has 2 wavelengths. This deficiency is in part overcome by using the Feature Type Score derived from the cloud-aerosol discrimination algorithm (Yorks et al. 2015; NASA CATS Group 2018), which is discussed in more detail later in this study.

One of the traditional parameters used to quantify atmospheric aerosols is Aerosol Optical Depth, or AOD. AOD quantifies the amount of attenuation of light through an aerosol layer (Kaufman 2002).

Using two years of observations from CATS, this study focuses on understanding the following questions: How well do CATS derived AOD and aerosol vertical distributions compare with aerosol properties derived from other ground-based and satellite

observations such as AERONET, MODIS and CALIOP? Do differences exhibit a diurnal cycle? What are the diurnal variations of aerosol optical depth on a global domain? What are the diurnal variations of aerosol vertical distribution on both regional and global scales?

Chapter 2

Data and Methodology

Three datasets, including ground-based AERONET data, as well as satellite retrieved aerosol properties from MODIS and CALIOP, are used for inter-comparing with AOD and aerosol vertical distributions from CATS. Upon thorough evaluation and quality assurance procedures, CATS data are further used for studying diurnal variations of AOD and aerosol vertical distributions for the period of Mar. 2015 – Oct. 2017.

2.1 CATS

The primary quantity measured by CATS is the total attenuated backscatter, which is further converted to aerosol extinction and AOD through a lidar retrieval process (Yorks et al. 2015). To do this, molecular backscatter must be calculated and removed, leaving particulate backscatter from aerosols. The relation between the particulate backscatter and aerosol extinction is defined as follows:

$$\sigma_p(z) = S_p \beta_p(z) \quad (1)$$

Where $\sigma_p(z)$ is the particulate extinction, S_p is the extinction to backscatter ratio, or lidar ratio, and $\beta_p(z)$ is the particle backscatter. The AOD, τ , can then be calculated as follows:

$$\tau = \int_{z_b}^{z_t} \sigma_p(z) dz \quad (2)$$

Where z_b and z_t are the bottom and top of the particulate layers, respectively (Yorks et al. 2015; Weitkamp 2006).

As is clear from this equation, a major source of uncertainty is the assumption of the lidar ratio, or S_p . The default lidar ratios are taken from look-up tables of values

retrieved from years of aircraft lidar data by aerosol type. Aerosol type, in turn, is determined using the cloud-aerosol discrimination algorithm (Yorks et al. 2015).

The CATS cloud-aerosol discrimination (CAD) algorithm is a multidimensional probability density function (PDF) technique that is based on the CALIOP algorithm (Liu et al. 2009). The PDFs were developed based on Cloud Physics Lidar (CPL) measurements obtained during over 11 field campaigns in 10 years. In this way, aerosol type can be determined based on various thresholds in the lidar data, which can then be used to determine an appropriate lidar ratio. Although CATS and CALIOP employ similar methods to derive extinction and AOD from measured lidar backscatter, it should be noted that they do not use the same default lidar ratios. Also, because CATS does not have both a 532 nm and a 1064 nm wavelength, the ratio between these two wavelengths (i.e. color ratio) was not able to be used for discrimination between cloud and aerosol. Rather than using layer-integrated attenuated backscatter color ratio as in CALIOP, CATS uses thresholds of layer-integrated attenuated backscatter intensity and perpendicular backscatter to help discriminate between cloud and aerosol (Yorks et al. 2015; NASA CATS Group 2018).

CATS Level 2 (L2) Version 3-00 5 km Aerosol Profile products (L2O_D-M7.2-V3-00_05kmPro, L2O_N-M7.2-V3-00_05kmPro) were used in this study for nearly the entire period of CATS operation on the ISS (~Mar. 2015–Oct. 2017). CATS L2 profile data is provided at 5 km along-track horizontal resolution and 533 vertical levels at 60 m vertical resolution and a wavelength of 1064 nm. CATS also provides data at 532 nm, but due to a laser-stabilization issue, 532 nm data is not recommended for use (Yorks et al. 2016). Thus, only 1064 nm products were used in this study. Although the uncertainties

in CATS aerosol retrievals have not yet been documented for the CATS V3-00 AOD products, much like CALIOP, uncertainties in the calibration and assumed lidar ratios are the primary contributors. Thus far, the uncertainty in the CATS 1064 nm attenuated total backscatter (ATB) has been reported on the order of 7-10% for nighttime and around 20% for daytime (Pauly et al. 2019).

CATS data are quality-assured following a manner similar to Campbell et al. (2012), which was applied to CALIOP. Quality assurance thresholds (including extinction QC flag, Feature Type Score, and uncertainty in extinction coefficient) are listed below:

(a) Extinction_QC_Flag_1064_Fore_FOV is equal to 0 (non-opaque layer; lidar ratio unchanged)

(b) Feature_Type_Fore_FOV = 3 (contains aerosols only)

(c) $-10 \leq \text{Feature_Type_Score_FOV} \leq -2$ (Feature Type Score < 0 is aerosol, with -10 being complete confidence, and 0 being as likely to be cloud as aerosol)

(d) Extinction_Coefficient_Uncertainty_1064_Fore_FOV $\leq 10 \text{ km}^{-1}$

Extinction was also constrained using a cap as provided in the CATS data catalog (Extinction_Coefficient_1064_Fore_FOV $\leq 1.25 \text{ km}^{-1}$), similar to several previous studies (Redemann et al. 2012; Toth et al. 2016). Only profiles with individual extinction coefficient values less than 1.25 km^{-1} are included in this study. Small negative extinction coefficient values, however, are included in aerosol profile related analysis, to reduce potential high biases in computed mean profiles. Note that a similar approach has also been conducted in deriving passive-based AOD climatology (e.g. Remer et al. 2005). For this study, both the Aerosol_Optical_Depth_1064_Fore_FOV and Extinction_Coefficient_1064_Fore_FOV datasets were used to provide AOD and 1064 nm

extinction profiles (hereafter the term “extinction” will refer to 1064 nm unless explicitly stated otherwise), respectively.

2.2 AERONET

By measuring direct and diffuse solar energy, AERONET observations are used for retrieving AOD and other ancillary aerosol properties such as size distributions (Holben et al. 1998). To convert solar energy measurements to AOD (τ), Beer’s Law is utilized:

$$I = I_0 e^{-\tau} \quad (3)$$

where I is the solar radiation intensity measured by the photometer and I_0 is the intensity of solar radiation at the top of the atmosphere.

AERONET data are considered the ground truth for evaluating CATS retrievals in this study. Only cloud screened and quality assured version 3 level 2 AERONET data at the 1020 nm spectrum are selected and are used for inter-comparing with CATS AOD retrievals at the 1064 nm wavelength. AERONET does not have specific guidance on error in the 1020 nm channel, as it is known to have some thermal sensitivities. However, it does report significantly more confidence in version 3 of the data, which has temperature correction (Giles et al. 2019). Error models are ongoing, and for this study we assumed double the RMSE, or +/-0.03. Note that version 3 AERONET data are designed to reduce thin cirrus cloud contamination as well as rescue heavy aerosol scenes that were misclassified as clouds in previous versions (e.g., Giles et al. 2019).

2.3 MODIS Collection 6.1 Dark Target product

Moderate Resolution Imaging Spectroradiometer (MODIS) Aqua and Terra Collection 6.1 Dark Target over-ocean AOD data (Levy et al. 2013) were used for comparison to CATS AOD. Because MODIS is not an active sensor like CATS and CALIOP, and is also not a ground-based sensor like AERONET, it utilizes a different method to calculate AOD. A look-up table is formed by using a radiative transfer model to compute satellite radiances as functions of observing conditions for each available wavelength for different aerosol modes and different optical depths. Over oceans, the MODIS algorithm compares observed radiances and matches them to modeled radiances in the look-up table, comparing them across all wavelengths for different values of optical depth and mode until a combination is found that produces the minimum error between the observed and modeled radiances (Remer 2005).

The data field of `Effective_Optical_Depth_Best_Ocean` was used and only those data flagged as “good” or “very good” by the `Quality_Assurance_Ocean` runtime QA flags were selected for this study, similar to Toth et al. (2018). Because MODIS does not provide AOD in the 1064 nm wavelength, AOD retrievals from 860 and 1240 nm spectral channels are used to logarithmically interpolate AODs at 1064 nm. Here we assume the Ångström Exponent value, computed using instantaneous AOD retrievals at 860 and 1240 nm, remains the same for the 860 to 1064 nm wavelength range, similar to what has been suggested by Shi et al. (2011; 2013). Mean and standard deviation of Ångström exponents using this method were 0.69 and 0.55, respectively. Only totally cloud free (or cloud fraction equal to zero) retrievals, as indicated by the `Cloud_Fraction_Land_Ocean` parameter, are used. While the uncertainties in MODIS infrared (e.g. 1240 nm) retrievals

are less explored, the reported over ocean MODIS DT AOD expected error envelopes are $(+(0.04 + 0.1 \cdot \text{AOD}), -(0.02 + 0.1 \cdot \text{AOD}))$ for the green channel (Levy et al. 2013).

2.4 CALIOP

NASA's CALIOP is an elastic backscatter lidar that operates at both 532 nm and 1064 nm wavelengths (Winker et al. 2009). Being a part of the A-Train constellation (Stephens et al. 2002), CALIOP provides both day- and night-time observations of Earth's atmospheric system, at a sun-synchronous orbit, with a laser spot size of around 70 m and a temporal resolution of ~ 16 days (Winker et al. 2009). For this study, CALIOP Level 2.0 Version 4.1 5 km Aerosol Profile products (L2_05kmAProf) are used for inter-comparing to CATS retrieved AODs and aerosol vertical distributions.

L2_05kmAProf data are available at 5 km horizontal resolution along-track and include aerosol retrievals at both 532 nm and 1064 nm wavelengths. The vertical resolution is 60 m near-surface, degrading to 180 m above 20.2 km in MSL altitude. As only 1064 nm CATS data are used in this study as mentioned above, likewise only those CALIOP parameters relating to 1064 nm are used in this study (Vaughan et al. 2019; Omar et al. 2013). Note that as suggested by Rajapakshe et al. (2017), lower signal-to-noise ratio (SNR) and higher minimum detectable backscatter are found for the CALIOP 1064 nm data in-comparing with the CALIOP 532 nm data. Also, the CALIOP aerosol layers are detected at 532 nm and the 1064 nm extinction is only computed for the bins within these layers. This may introduce a bias for aerosol above cloud studies. The uncertainty in retrieved aerosol extinction, as suggested by Young et al. (2013), is around $0.05\text{--}0.5 \text{ km}^{-1}$ for the 532 nm channel. Validated against AERONET data, Omar et al. (2013) suggested

that 74% and 81% of the CALIOP AOD retrievals fall within the expected uncertainties ($0.05+0.4*AOD$) as suggested by Winker et al. (2009) for the 1064nm channel, for all sky and clear sky conditions, respectively.

In this study, `Extinction_Coefficient_1064` and `Column_Optical_Depth_Tropospheric_Aerosols_1064` are used for CALIOP extinction and AOD retrievals, respectively (Vaughan et al. 2019; Omar et al. 2013). As with the CATS data, CALIOP data are quality-assured following the quality assurance steps as mentioned in a few previous studies (e.g., Campbell et al. 2012; Toth et al. 2016; 2018). These QA thresholds are listed below:

- (a) `Extinction_QC_Flag_1064` is equal to 0 (unconstrained retrieval; initial lidar ratio unchanged)
- (b) `Atmospheric_Volume_Description` = 3 or 4 (contains aerosols only)
- (c) $-100 \leq CAD_Score \leq -20$ ($CAD < 0$ is aerosol, with -100 being complete confidence, and 0 being as likely to be cloud as aerosol)
- (d) `Extinction_Coefficient_Uncertainty_1064` $\leq 10 \text{ km}^{-1}$

Furthermore, as in Campbell et al. (2012), only those profiles with $AOD > 0$ were retained in order to avoid profiles composed of only retrieval fill values. Extinction was also constrained to the nominal range provided in the CALIOP data catalog (`Extinction_1064` $\leq 1.25 \text{ km}^{-1}$), similar to our QA procedure for CATS as described above.

2.5 Collocation Methodology

2.5.1 AERONET

As the initial check, CATS data from nearly the entire mission (Mar. 2015-Oct. 2017) were spatially (within 0.4 degree latitude and longitude) and temporally (± 30 minutes) collocated against ground-based AERONET data. Note that one AERONET measurement may be associated with several CATS retrievals in both space and time, and vice versa. Thus, both CATS and AERONET data were further averaged spatially and temporally, which results in only one pair of collocated and averaged CATS and AERONET data for a given collocated incident. Also, only data pairs with AOD larger than 0 from both instruments are used for the analysis. This step is necessary to exclude CATS profiles with all retrieval fill values (Toth et al. 2018). Such profiles containing all retrieval fill values were found to make up approximately 5.3% of all CATS profiles in the dataset. Note that the CATS-AERONET comparisons are for daytime only, and higher uncertainties are expected for CATS daytime than nighttime AODs.

2.5.2 MODIS

To examine over ocean performance, column integrated CATS AODs are inter-compared with collocated Terra and Aqua C6.1 MODIS DT over ocean AOD, interpolated to 1064 nm. Over ocean C6.1 MODIS DT data are selected due to the fact that higher accuracies are reported for over ocean versus over land MODIS DT AOD retrievals (Levy et al. 2013). In addition, compared to over land MODIS DT data, which provide AOD retrievals at three discrete wavelengths (0.46, 0.55 and 0.65 μm), over water AOD retrievals are available from 7 wavelengths including the 0.87 and 1.24 μm spectral

channels, allowing a comparison with CATS AOD at the same wavelength upon logarithmic interpolation, again, assuming the aerosol Ångström Exponent value remains unchanged from 0.87 μm to 1.064 μm as well as from the 1.064 μm to 1.24 μm spectral channels. MODIS and CATS AOT retrievals are collocated for the study period of Mar. 2015-Oct. 2017. Pairs of CATS and MODIS data were first selected for both retrievals that fall within ± 30 minutes and 0.4 degrees latitude and longitude of each other. Then, similar to the AERONET and CATS collocation procedures, collocated pairs were further averaged to construct one pair of collocated MODIS and CATS data for a given collocation incident. More discussion of the impact of the chosen spatial and temporal thresholds is included in section 3.3.

2.5.3 CALIOP

Again, for each collocation incident, pairs of CALIOP and CATS data are selected in which both retrievals fall within ± 30 minutes temporally and 0.4 degrees latitude and longitude spatially. There could be multiple CATS retrievals corresponding to one CALIOP data point, and vice versa. Thus, the collocated pairs are further averaged in such a way that only one pair of collocated CATS and CALIOP data is derived for each collocation incident.

One advantage of CATS is its ability to retrieve both column-integrated AOD and vertical distributions of aerosol extinction. Therefore, in addition to AOD, extinction profiles from CATS are compared with that from CALIOP. Again, similar to the collocation of CALIOP AOD, collocated vertical profiles for CATS and CALIOP are first found for both retrievals that are close in space and time (within ± 30 minutes and 0.4 degrees latitude and longitude). However, different from the AOD collocation, only one

pair of collocated CATS and CALIOP profiles, which has the closest Euclidian distance on the earth's surface, is retained for each collocated incident.

Chapter 3

Results and Discussion

Note that most evaluation efforts for passive and active sensor AOD retrievals are focused on the visible spectrum and the performance of AOD retrievals at the 1064 nm channel is less explored. Thus, in this sub-section, the performance of over land and over ocean CATS AOD retrievals are compared against AERONET and C6.1 over ocean MODIS Dark Target (DT) aerosol products. In AOD related studies, CATS and CALIOP reported AOD values are used. However, only AOD values with corresponding aerosol vertical extinction that meet the QA criteria as mentioned in Sections 2.1 and 2.4 were used. CATS derived aerosol extinction vertical distributions are also cross-compared against collocated CALIOP aerosol extinction vertical distributions.

3.1 CATS-AERONET

Without quality-assurance procedures, high spikes in CATS AOD of above 1 can be found for collocated AERONET data with AOD less than 0.4 (Figure 1a). Still, high spikes in CATS AOD are much reduced compared to the V2-01 CATS aerosol products (e.g., a similar plot as Figure 1 is included in the Appendix A with the use of V2-01 CATS aerosol data). Upon completion of the QA steps as outlined in Section 2.1, reasonable agreement is found between quality-assured CATS (1064 nm) vs. AERONET (1020 nm) AODs with a correlation of 0.65 (Figure 1b). Comparing Figure 1a with 1b, with the loss of only ~1-2% of collocated pairs due to the QA procedures, there is an overall improvement in correlation between CATS and AERONET AOD from 0.51 to 0.64, thus, only quality-assured CATS data are used hereafter. It was also found that requiring the

Extinction QC flag to be equal to 0 and the Extinction Uncertainty to be less than 10 km^{-1} had the largest impacts on reducing the difference in mean and medians of the AERONET and CATS AOD. This exercise highlights the need for careful quality checks of the CATS data to overcome cloud-aerosol discrimination uncertainties before applying the CATS data to advanced applications.

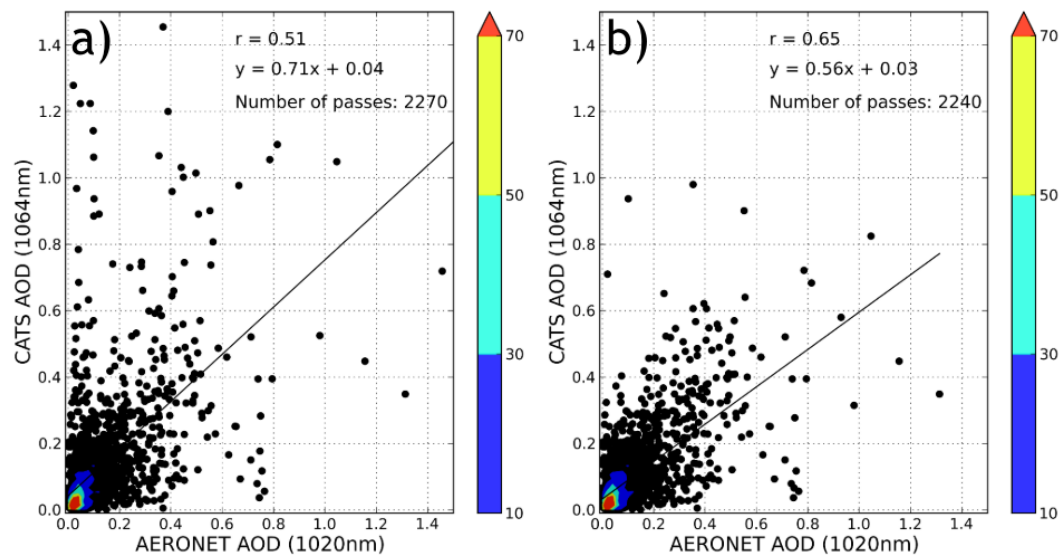


Figure 1: Collocated AERONET 1020 nm AOT vs. CATS 1064 nm AOD a) without CATS QA applied, and b) with CATS QA applied.

3.2 CATS-MODIS

A comparison of MODIS and CATS AOD is shown in Figure 2. A correlation of 0.72 is found between collocated over water Terra MODIS C6.1 DT and CATS AODs with a slope of 0.74 (Figure 2a). Similar results are found for the comparisons between over

water Aqua MODIS and CATS AODs with a correlation of 0.74 and a slope of 0.70 (Figure 2b), indicating reasonable agreement between CATS and MODIS AOD.

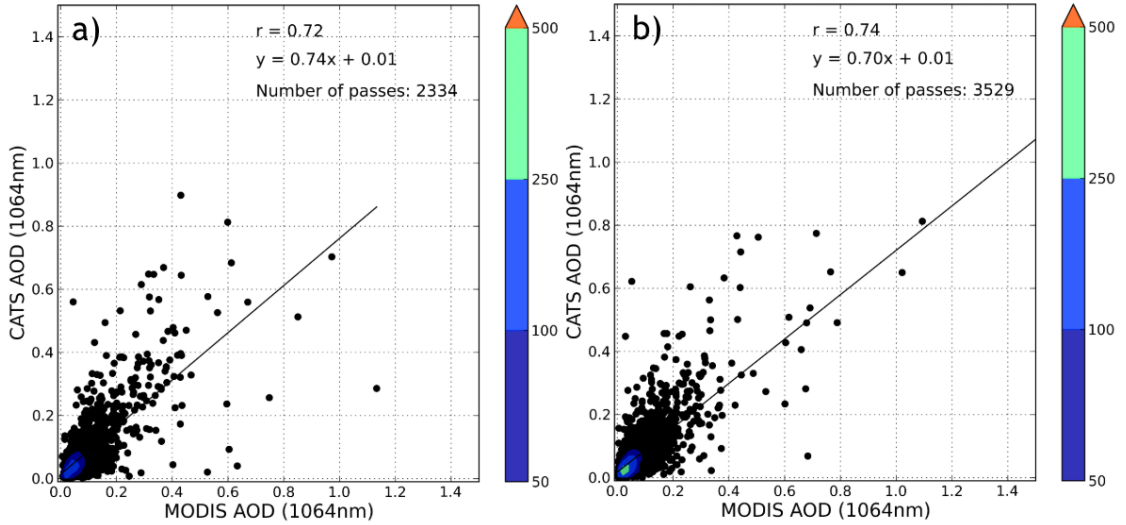


Figure 2: Collocated MODIS C6.1 a) Terra and b) Aqua interpolated 1064 nm AOD vs. CATS 1064 nm AOD with CATS QA applied.

3.3 CATS-CALIOP AOD

In the previous two sections, AODs from CATS were inter-compared with retrievals from passive-based sensors such as MODIS and AERONET. In this section, AOD data from CALIOP, which is an active sensor, are evaluated against AOD retrievals from CATS. Note that despite difference in instrumental designs, CALIOP and CATS are both elastic backscatter lidars, meaning that they derive aerosol properties in a similar manner.

Figure 3a shows the comparison of CATS and CALIOP AODs for all collocated pairs including both day- and night-time. A reasonable correlation of 0.74, with a slope of 0.73, is found for a total of 2762 collocated data pairs. Further breaking down the comparison into day and night cases, a better agreement is found between the two datasets

during nighttime with correlations of 0.81 and 0.83 for over-ocean and over-land cases respectively. In comparison, a lower correlation of 0.64, with a slope of 0.49, is found between the two datasets, using over land daytime data only, for a total of 170 collocated pairs. Correspondingly, a lower correlation of 0.55, with a slope of 0.57, is found between the two datasets, using over ocean daytime data only, for a total of 1180 collocated pairs. This result is not surprising as daytime data from both CALIOP and CATS are noisier due to solar contamination (e.g. Omar et al. 2013; Toth et al. 2016).

Note that based on the slopes of the regression lines shown in Figures 1-3, AODs retrieved by CATS are less than AERONET, CALIOP and DT Aqua MODIS AOD retrievals. As shown in Table 1, however, for the one-to-one collocated datasets, mean CATS AODs (1064 nm) are ~10% higher than AERONET AODs (1020 nm). The CATS AODs are ~3% higher than CALIOP AOD (1064 nm) and are ~5-10% higher than DT MODIS AODs. One possible explanation for this discrepancy is because mean AODs are dominated by low AOD cases and the slopes of the regression relationships are strongly affected by a few high AOD cases. Thus, it is likely that CATS AODs are overestimated at the low AOD ranges and are underestimated at the high AOD ranges.

As suggested by Omar et al. (2013), the choices of spatial and temporal collocation windows have an effect on collocation results. Thus, the exercises in Figures 1-3 were repeated by doubling the spatial and temporal collocation windows as well as reducing the collocation windows by half. The descriptive statistics of this sensitivity study are included in Table 2. While the number of collocated data pairs are drastically affected by the spatial and temporal collocation window sizes, less significant changes are found in descriptive statistics such as mean, median, and standard deviations of AODs, as well as slopes and

correlation values. The slope of DT Aqua MODIS and CATS AODs, however, seems sensitive to changes in collocation methods. Changes in slope of 0.61 to 0.78 are found for the change of temporal collocation window from 15 minutes to 60 minutes with a fixed spatial collocation window of 0.4° latitude/longitude.

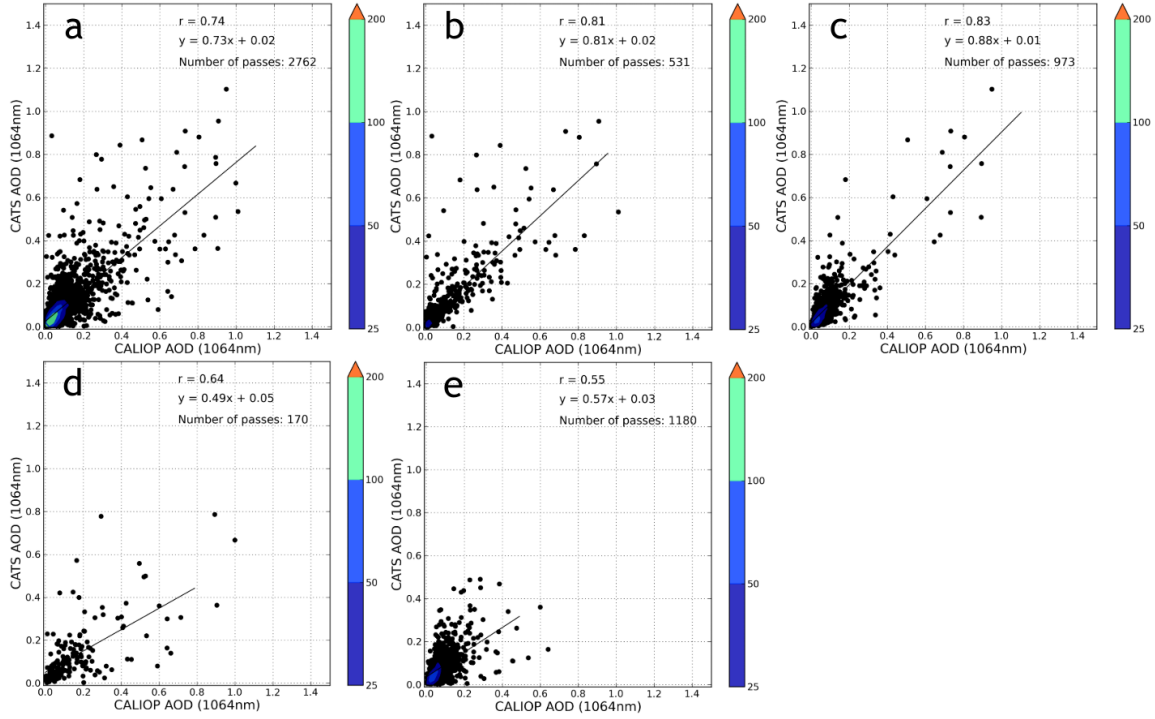


Figure 3: Collocated CALIOP 1064 nm AOD vs. CATS 1064 nm AOD with CATS QA applied for a) both day and night, b) nighttime over-land, c) nighttime over-water, d) daytime over-land, e) daytime over-water.

Table 1: Descriptive statistical properties between collocated CATS and AERONET, CALIOP and Aqua MODIS AOD retrievals. Here STDDEV indicates standard deviation of AOD and R-value represents the correlation coefficient.

Sensor	No. of Points	Slope	R-value	Mean AOD	Median AOD	Max AOD	Min AOD	STDDEV	CATS Mean AOD	CATS Median AOD	CATS Max AOD	CATS Min AOD	CATS STDDEV
AERONET	2240	0.56	0.65	0.088	0.054	0.98	0.001	0.103	0.099	0.058	1.31	0.0004	0.119
MODIS Aqua	3529	0.7	0.74	0.067	0.048	0.81	0.0004	0.07	0.097	0.053	1.76	0.002	0.075
MODIS Terra	2334	0.74	0.72	0.076	0.056	0.9	0.0013	0.081	0.084	0.065	1.13	0.0063	0.079
CALIOP	2762	0.74	0.74	0.089	0.063	1.01	0	0.102	0.092	0.065	1.1	0.0018	0.1

Table 2: Sensitivity study of descriptive statistical properties between collocated CATS and AERONET, CALIOP and Aqua MODIS AOD retrievals by varying spatial and temporal collocation windows. Here STDDEV indicates standard deviation of AOD and R-value represents the correlation coefficient.

Collocation Thresholds	AERONET/CATS			AERONET							CATS							
	No. of Points	Slope	R-value	Mean AOD	Median AOD	Max AOD	Min AOD	STDDEV	Mean AOD	Median AOD	Max AOD	Min AOD	STDDEV	Mean AOD	Median AOD	Max AOD	Min AOD	STDDEV
Spatial (30 min.)	0.2°	0.54	0.63	0.092	0.052	0.82	0.002	0.107	0.102	0.058	1.31	0.0004	0.124	0.092	0.052	1.74	0.003	0.075
	0.4°	0.56	0.65	0.088	0.054	0.98	0.001	0.103	0.099	0.058	1.31	0.0004	0.119	0.092	0.053	1.76	0.002	0.075
	0.8°	0.53	0.63	0.087	0.052	0.98	0.001	0.105	0.097	0.055	2	0.0004	0.125	0.092	0.053	1.71	0.003	0.073
Temporal (0.4° lat./lon.)	15 minutes	0.54	0.63	0.089	0.053	0.98	0.001	0.105	0.1	0.057	1.34	0.0004	0.123	0.092	0.052	1.76	0.003	0.078
	30 minutes	0.56	0.65	0.088	0.054	0.98	0.001	0.103	0.099	0.058	1.31	0.0004	0.119	0.092	0.053	1.76	0.002	0.075
	60 minutes	0.55	0.64	0.087	0.053	0.98	0.001	0.103	0.098	0.057	1.32	0.0004	0.118	0.092	0.054	1.76	0.003	0.074
Collocation Thresholds Spatial (30 min.)	CALIOP/CATS			CALIOP							CATS							
	No. of Points	Slope	R-value	Mean AOD	Median AOD	Max AOD	Min AOD	STDDEV	Mean AOD	Median AOD	Max AOD	Min AOD	STDDEV	Mean AOD	Median AOD	Max AOD	Min AOD	STDDEV
	1948	0.73	0.76	0.088	0.063	1.15	0	0.104	0.092	0.065	1.12	0.0013	0.1	0.092	0.065	1.12	0.0013	0.1
2762	0.74	0.74	0.089	0.063	1.01	0	0.102	0.092	0.065	1.1	0.0018	0.1	0.092	0.065	1.1	0.0018	0.1	
5070	0.80	0.74	0.089	0.063	0.94	0	0.099	0.093	0.066	1.61	0.0008	0.107	0.092	0.066	1.61	0.0008	0.107	
Temporal (0.4° lat./lon.)	15 minutes	0.76	0.77	0.09	0.063	0.95	0	0.104	0.092	0.066	1.1	0.0024	0.102	0.092	0.066	1.1	0.0024	0.102
	30 minutes	0.74	0.74	0.089	0.063	1.01	0	0.102	0.092	0.065	1.1	0.0018	0.1	0.092	0.065	1.1	0.0018	0.1
	60 minutes	0.74	0.75	0.09	0.063	1.4	0	0.104	0.093	0.066	1.55	0.0007	0.103	0.092	0.066	1.55	0.0007	0.103
Collocation Thresholds Spatial (30 min.)	MODIS Aqua/CATS			MODIS Aqua							CATS							
	No. of Points	Slope	R-value	Mean AOD	Median AOD	Max AOD	Min AOD	STDDEV	Mean AOD	Median AOD	Max AOD	Min AOD	STDDEV	Mean AOD	Median AOD	Max AOD	Min AOD	STDDEV
	2998	0.73	0.75	0.062	0.043	0.86	0.0004	0.073	0.07	0.052	1.74	0.003	0.075	0.07	0.052	1.74	0.003	0.075
3529	0.7	0.74	0.067	0.048	0.81	0.0004	0.07	0.07	0.053	1.76	0.002	0.075	0.07	0.053	1.76	0.002	0.075	
4107	0.67	0.74	0.07	0.053	0.79	0.0004	0.066	0.071	0.053	1.71	0.003	0.073	0.07	0.053	1.71	0.003	0.073	
Temporal (0.4° lat./lon.)	15 minutes	0.61	0.71	0.064	0.048	0.82	0.0004	0.067	0.069	0.052	1.76	0.003	0.078	0.069	0.052	1.76	0.003	0.078
	30 minutes	0.70	0.74	0.067	0.048	0.81	0.0004	0.07	0.07	0.053	1.76	0.002	0.075	0.07	0.053	1.76	0.002	0.075
	60 minutes	0.78	0.76	0.069	0.049	1.21	0.0004	0.076	0.072	0.054	1.76	0.003	0.074	0.072	0.054	1.76	0.003	0.074

Still, larger discrepancies between CATS and CALIOP AODs during daytime indicate that both sensors are susceptible to solar contamination. To overcome solar contamination and more accurately detect aerosol layers, CALIOP and CATS data products are averaged up to 80 km and 60 km, respectively. Noel et al. (2018) found that the feature type score can be used for cloud screening throughout the diurnal envelope of solar angles. To further evaluate impact of the solar contamination introduced bias in the diurnal analysis in aerosol detection or products, CATS AODs are evaluated as a function of local time. For each CATS observation of a given location and UTC time, the associated local time is computed by adding the UTC time by 1 hour per 15° longitude away from the Prime Meridian in the east direction. Figure 4a shows the CATS AOD versus local time for both global land and oceans, constructed using 6 hourly mean CATS AOD binned on a 5 degree by 5 degree grid globally. While the data has additional noise, no major deviations in AODs are found during either sunrise or sunset time, although we speculate that larger uncertainties in CATS AODs and extinctions may be present around day and night terminators. Figure 4b shows a similar plot as Figure 4a, but with the region restricted to 25°S-52°S. Here, variations in CATS AODs are investigated as a function of local time, over relatively aerosol free oceans. 25°S was picked as the cutoff line as CATS data only available to 51.6°S (limited to the ISS inclination angle) and thus, this threshold is used to ensure enough data samples in the analysis, although some land regions are also included. As indicated in Figure 4b, again, no significant deviations in pattern are found for both sunrise and sunset time, plausibly indicating that solar contamination, as speculated, may not be as significant. Comparing the mean AOD at local midnight to the mean AOD at

local noon by performing a student's t test, the difference is not significant at the 95% confidence level, with a p-value of 0.16.

Figure 4c shows the difference between AERONET (1020 nm) and CATS (1064 nm) AOD (Δ AOD) as a function of local time. Again, although data are rather noisy, no major pattern is found near sunrise or sunset times, further indicating that solar contamination during dawn or dusk times may have a less severe impact to CATS AOD retrievals from a long term mean perspective. In summary, Sections 3.1-3.3 suggest that with careful QA procedures, AOD retrievals from CATS are comparable to those from other existing sensors such as AERONET, MODIS, and CALIOP at the same local times.

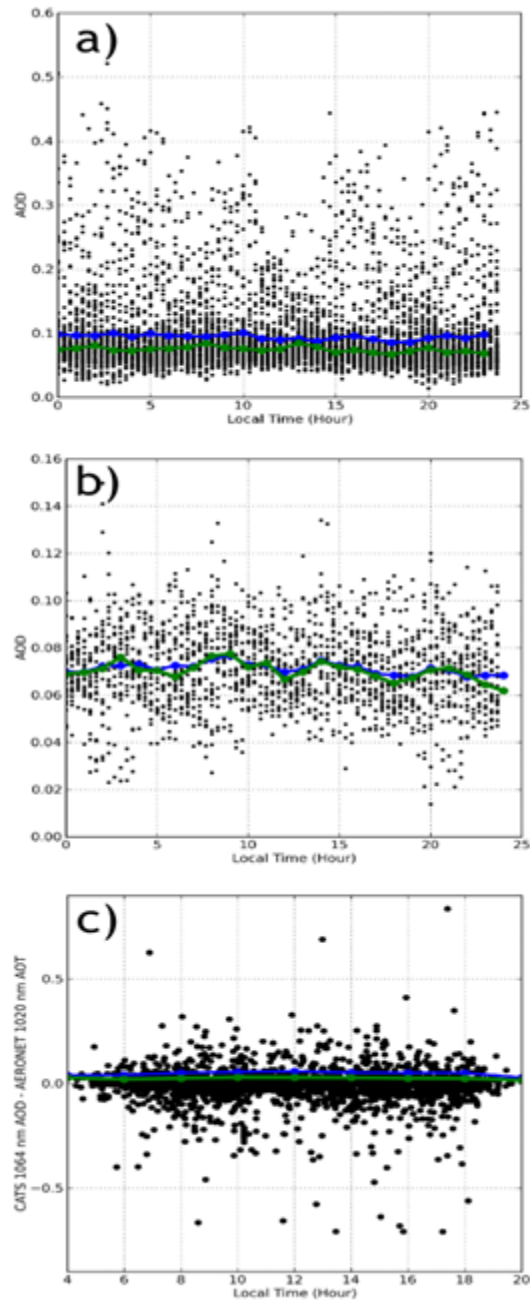


Figure 4: CATS 1064 nm AOD a) as a function of local time for the globe, and b) as a function of local time for areas south of -25 degrees. The difference between CATS 1064 nm AOD and AERONET 1020 nm AOD as a function of local time is shown in c). The mean is represented by the blue line, while the median is the green line.

3.4 CATS-CALIOP Vertical Extinction Profiles

In this section, the vertical profiles of extinction are compared between collocated CATS and CALIOP pairs. As shown in Figure 5e, a reasonable agreement is found between CATS V3-00 aerosol extinction with CALIOP for over land. However, CATS overestimates aerosol extinction around 1 km compared to CALIOP over ocean (Figure 5d). This can also be seen on a plot of the difference between CATS and CALIOP 1064 nm extinction for all collocated profiles, included in Figure 5f, where there is an overall positive difference around 1 km.

Due to the precessing orbit of the ISS, the CATS sampling is irregular and different compared to the sun-synchronous orbits of the A-Train sensors. These orbital differences between CATS and CALIOP make comparing the data from these two sensors challenging since they are fundamentally observing different locations of the Earth at different times. Thus, we shouldn't expect the extinction profiles and AOD from these two sensors to completely agree. Additionally, there are other algorithm and instrument differences that can lead to differences in extinction coefficients and AOD. Over land where dust is the dominant aerosol type, differences in lidar ratios between the two retrieval algorithms (CATS uses 40 sr while CALIOP uses 44 sr), can cause CATS extinction coefficients that are up to 10% lower than CALIOP, potentially explaining the higher CALIOP extinction values in Figure 5e. Over ocean, especially during daytime, differences in CATS and CALIOP lidar ratios for marine and smoke aerosols can introduce a difference between CATS and CALIOP extinction coefficients (Figure 5d). These difference in over ocean data (Figure 5d) could also attributed to differences in CATS and CALIOP 1064 nm backscatter calibration. For example, Pauly et al. (2019) reports that CATS attenuated total

backscatter is about 19.7% lower than PollyXT ground-based lidar measurements in the free troposphere and 19% lower than CALIOP opaque cirrus clouds due to calibration uncertainties for both sensors.

Also, differences in the lowest 250 m between CATS and CALIOP extinction profiles are observable, which are due to how the instrument algorithms detect the surface and near-surface aerosols. Both the CATS and CALIOP feature detection algorithms create a gap between the surface and near-surface aerosol base altitude, despite the possible presence of aerosols in this altitude region. CALIOP has an aerosol base extension algorithm that is designed to (1) detect scenarios when aerosols are present in the bins just above the surface and (2) extend the near-surface aerosol layer base down to the surface (Tackett et al. 2018). However, CATS does not use such an algorithm so false regions of “clear-air” exist between the surface and near-surface aerosol layers.

Vertical profiles of collocated CATS and CALIOP extinction for daytime only profiles and nighttime only profiles are shown in Figure 5b and 5c, respectively. Compared to a total collocated pair count of 2748 in the overall profile data, day and night profiles have 1311 and 1437 collocated pairs, respectively. Again, the shapes of the CATS and the CALIOP nm extinction vertical profile are similar for all three cases, despite the above mentioned offsets in altitude. Figure 5d and 5e show the mean of those extinction profiles which occurred over-water and over-land, as defined by the CATS surface type flag. Again, in both cases, CATS and CALIOP have similar shapes in their vertical extinction profiles. The vertical structure of over-water extinction is also very similar to that of all profiles, day, and night, which is perhaps not surprising as water profiles made up 2142 of 2748 (~78%) collocated pairs. The vertical structure of over-land is different from the

other groups, as the extinction is higher throughout a larger depth of the atmosphere, tapering off much more slowly from the surface. Furthermore, the extinction from CATS is actually lower than CALIOP for over-land profiles, unlike all other categories.

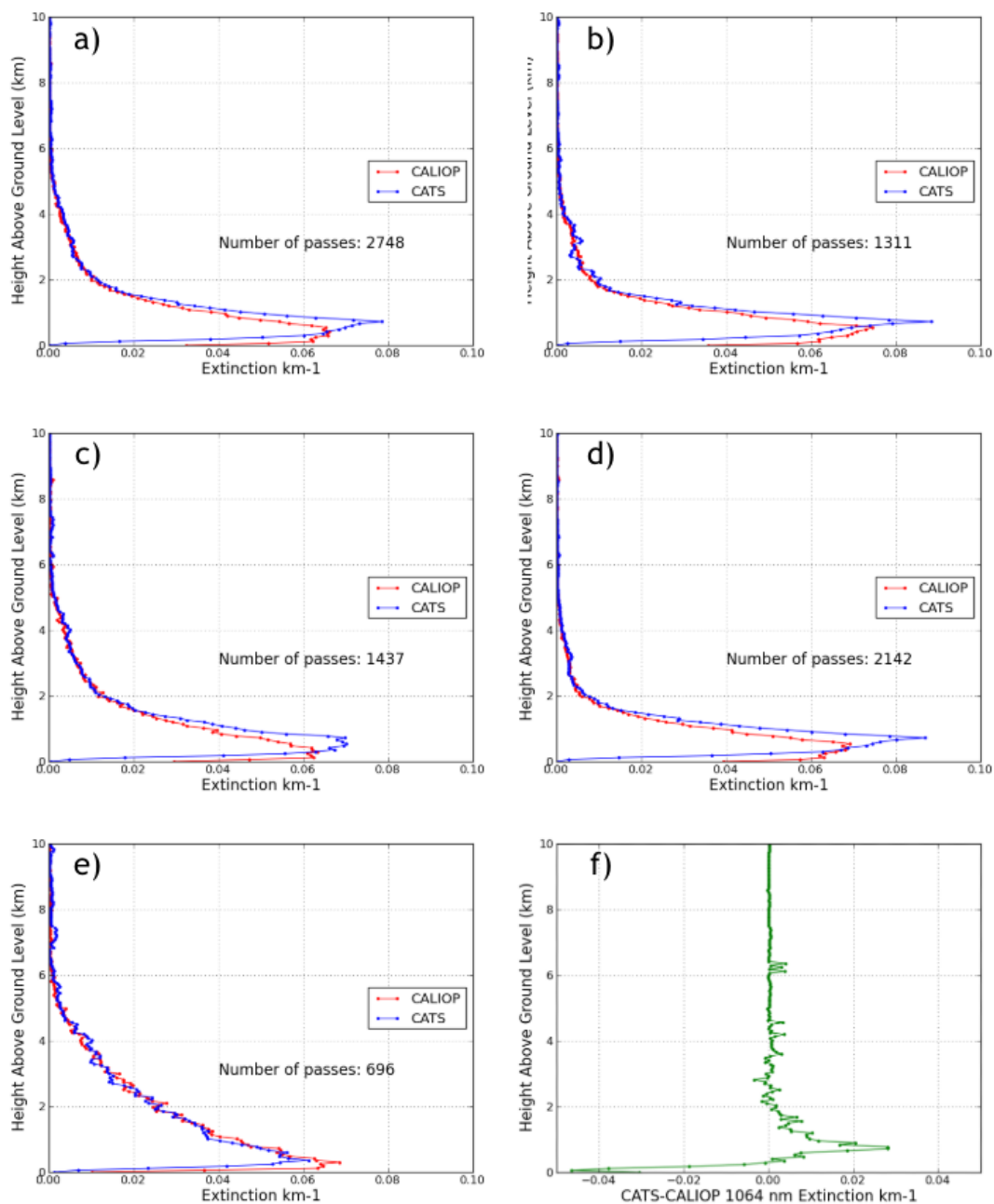


Figure 5: CATS and CALIOP vertical profiles of 1064 nm extinction for a) all profiles, b) daytime only, c) nighttime only, d) over-water, and e) over land. f) shows the difference between CATS and CALIOP mean 1064 nm extinction for all collocated profiles (5a) as a function of height. Mean AOD values are as follows: for CATS: a) 0.094, b) 0.091, c) 0.098, d) 0.088, e) 0.119, and for CALIOP: a) 0.093, b) 0.092, c) 0.093, d) 0.084, e) 0.127.

3.5 Application: Diurnal Cycle of AODs and Aerosol Vertical Distributions

Using the quality-assured CATS data, seasonal variations as well as diurnal variations in CATS AODs are derived in this section. Diurnal variations in the vertical distributions of CATS aerosol extinction are also examined at both global and regional scales.

3.5.1 Seasonal and Diurnal Variation of AOD

Figures 6a-b show the spatial distributions of CATS AODs at the 1064 nm spectral channel for boreal winter-spring (Dec.-May, DJFMAM) and boreal summer-fall (June-Nov., JJASON) seasons, for the period of Mar. 2015-Oct. 2017. To construct Figures 6a and 6b, quality assured CATS AODs are first binned on a 5 degree by 5 degree grid over the globe for the above mentioned two bi-seasons. For each $5 \times 5^\circ$ (latitude/longitude) bin, for a given season, CATS AODs are averaged on a pass-basis first, and then further averaged seasonally to represent AOD value of the given bin. Both daytime and nighttime retrievals are included in this Figure, as well as Figures 7-9.

In DJFMAM season, significant aerosol features are found over Africa-North, Middle East, India and Eastern China. For the JJASON season, besides the above mentioned regions, aerosol plumes are also observable over Africa-South, likely related to summer biomass burning of the region (e.g., Eck et al. 2013). The seasonal-based spatial distributions of AODs from CATS, although reported at the 1064 nm channel which is different from the 550 nm channel that is conventionally used, are similar to some published results (e.g., Lynch et al. 2016).

For comparison purposes, Figures 6c-6d shows similar plots to Figures 6a-6b, but with the use of CALIOP AOD at the 1064 nm spectral channel. Note that those are climatological means rather than pairwise comparisons. While patterns are similar in general, at regions with peak AODs of 0.4 or above for CALIOP, such as Africa-North for the DJFMAM season and Africa-North, Middle East and India for the JJASON, much lower AODs are found for CATS. In some other regions, such as over Africa-South for the JJASON season, however, higher CATS AOD values are observed. A table of mean AOD across each of these regions as well as over the globe (within the latitude range where CATS has data) has been included for reference (Tables 3). Figures 6e and 6f show similar spatial plots as Figures 6a and 6b but with the use of Aqua MODIS AODs from the DT products (using all available MODIS DT retrievals that passed QA steps as described in Section 2.3). For the Aqua MODIS DT products, aerosol retrievals at the short-wave infrared channels are only available over oceans, and thus Figures 6e-6f show only over ocean retrievals. Again, while general AOD patterns look similar, discrepancies are also visible, such as over the coast of southwest Africa for the JJASON season and over the west coast of Africa for the DJFMAM season. Those discrepancies may result from biases in each product, but it is also possibly due to the differences in satellite overpass times, as CALIOP provides early morning and afternoon over passes, and Aqua MODIS has an overpass time after local noon, while CATS is able to report atmospheric aerosol distributions at multiple times during a day.

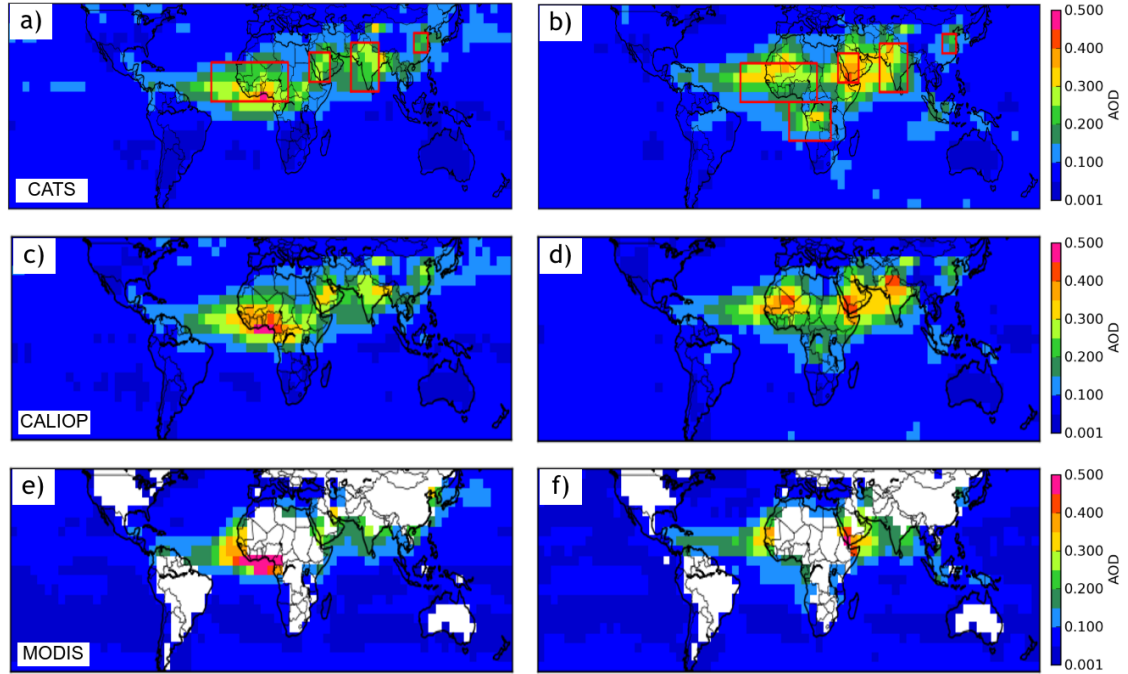


Figure 6: Mean AOD (1064 nm) by season for a) DJFMAM CATS, b) JJASON CATS, c) DJFMAM CALIOP, d) JJASON CALIOP, e) DJFMAM MODIS Aqua, and f) JJASON MODIS Aqua. Red boxes indicate locations of regional vertical distributions in Figures 12 and 13.

Table 3: CALIOP and CATS mean AODs / AOD standard deviations for regions as highlighted in Figure 6 and globally between +/- 52° latitude.

Region	Latitude	Longitude	Mean CATS AOD (DJFMAM/JJASON)	Mean CALIOP AOD (DJFMAM/JJASON)	Mean CATS Standard Deviation (DJFMAM/JJASON)	Mean CALIOP Standard Deviation (DJFMAM/JJASON)
Global	52°S-52°N	180°W-180°E	0.09/0.10	0.09/0.09	0.037/0.039	0.036/0.034
India	7.5°N - 32.5°N	65°E - 85°E	0.22/0.26	0.22 /0.28	0.068/0.072	0.072/0.078
Africa - North	2.5°N - 22.5°N	35°W - 20°E	0.25/0.24	0.30 /0.25	0.062/0.064	0.075/0.067
Africa - South	17.5°S - 2.5°N	0° - 30°E	0.12/0.20	0.15 /0.13	0.037/0.048	0.038/0.038
Middle East	12.5°N - 27.5°N	35°E - 50°E	0.23/0.35	0.26/0.35	0.076/0.099	0.082/0.091
China	27.5°N - 37.5°N	110°E - 120°E	0.20/0.17	0.21 /0.16	0.061/0.056	0.074/0.060

Similar to Figures 6a and 6b, Figures 7a and 7b show the spatial distribution of CATS AODs, but for CATS extinction values that are below 1 km Above Ground Level (AGL) only, for the DJFMAM and JJASON seasons respectively. Figure 7c and 7d show the CATS mean AOD plots for extinction values from 1-2 km AGL, while Figure 7e and

7f show CATS mean AOD for extinction values above 2 km AGL. For the DJFMAM season, elevated aerosol plumes with altitude above 2 km AGL are found over the Africa-North. For the JJASON season, elevated dust plumes (> 2 km AGL) are found over Africa-North and the Middle East regions, while elevated smoke plumes are found over the west coast of Africa-South where above cloud smoke plumes are often observed during the Northern hemispheric summer season (e.g., Alfaro-Contreras et al. 2016).

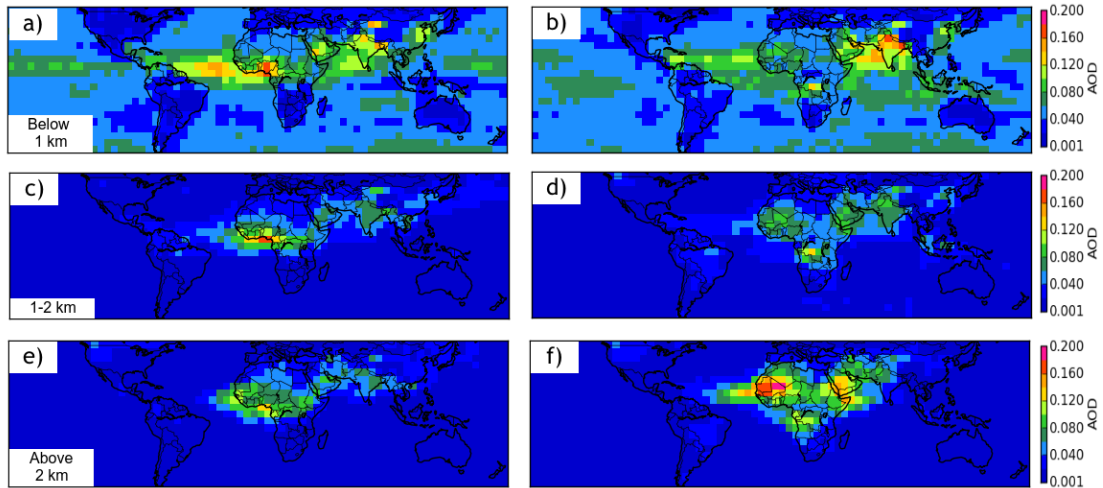


Figure 7: Mean CATS AOD (1064 nm) by season for a) DJFMAM below 1km AGL, b) JJASON below 1 km AGL, c) DJFMAM 1-2 km AGL, d) JJASON 1-2 km AGL, e) DJFMAM above 2 km AGL, and f) JJASON above 2 km AGL.

CATS has a non-sun-synchronized orbit, which enables measurements at nearly all solar angles. Thus, $5 \times 5^\circ$ (Latitude/Longitude) gridded seasonal averages (for DJFMAM and JJASON seasons) of CATS AODs at 0, 6, 12 and 18 UTC were constructed, representing 4 distinct times in a full diurnal cycle, as shown in Figure 8. To construct the seasonal averages, observations within ± 3 hours of a given UTC time as mentioned above are averaged to represent AODs for the given UTC time. On a global average, the mean AODs are 0.090, 0.089, 0.088 and 0.089 for 0, 6, 12 and 18 UTC respectively for the

JJASON season and are 0.099, 0.096, 0.093 and 0.093 for the DJFMAM season. Thus, no significant diurnal variations are found on a global scale.

Still, strong diurnal variations with the maximum averaged diurnal AOD changes of above 0.10 can be observed for regions with significant aerosol events such as Africa-North, Middle East and India for the DJFMAM season and Africa-North, Africa-South, Middle East and India for the JJASON season, as illustrated in Figure 9. Note that Fig. 9a shows the maximum minus minimum seasonal mean AODs for the four difference times as shown in Figs. 8a, c, e, g. Similarly, Fig. 9b shows the maximum minus minimum seasonal mean AODs for the four difference times as shown in Figs. 8b, d, f, h. Interestingly but not unexpectedly, regions with maximum diurnal variations match well with locations of heavy aerosol plumes as shown in Figures 6 and 8.

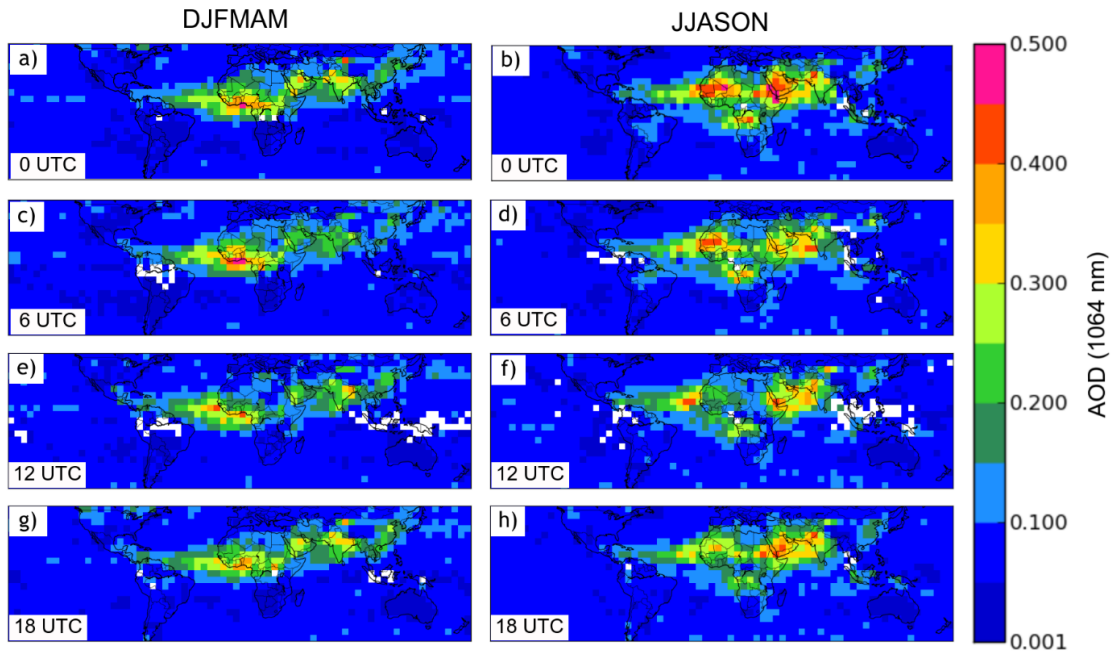


Figure 8: Seasonal Mean AOD (1064 nm) binned by every 6-hours for a) DJFMAM 0 UTC, b) JJASON 0 UTC, c) DJFMAM 6 UTC, d) JJASON 6 UTC, e) DJFMAM 12 UTC, f) JJASON 12 UTC, g) DJFMAM 18 UTC, and h) JJASON 18 UTC.

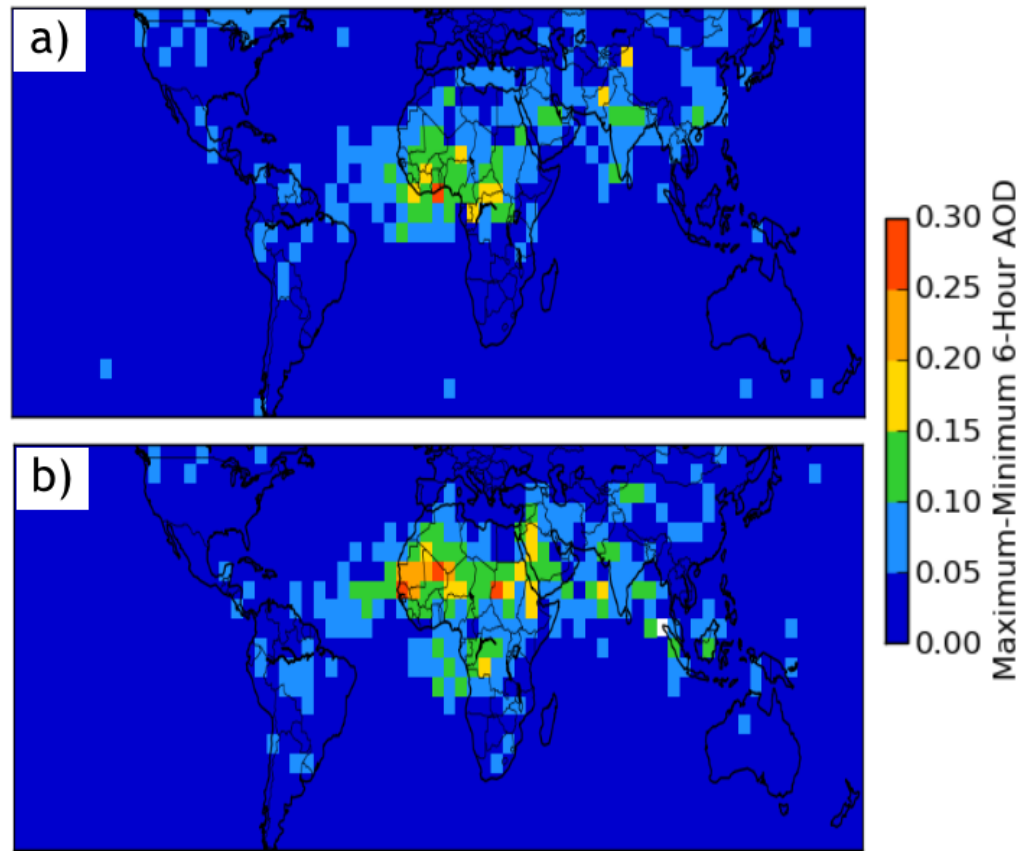


Figure 9: Maximum minus minimum mean seasonal AOD (1064 nm) for a) DJFMAM, and b) JJASON.

3.5.2 Diurnal variations of Aerosol Extinction on a Global Scale (both at UTC and local time)

Using quality assured CATS derived aerosol vertical distributions, mean global CATS extinction vertical profiles are also generated as shown in Figure 10. Similar to steps as described in the section 3.5.1, CATS extinction profiles are binned into 00, 06, 12, and 18 UTC times based on the closest match in time for the JJASON and DJFMAM seasons. Figure 10a shows the daily averaged CATS extinction profiles in a black line,

and 00, 06, 12 and 18 UTC averaged in blue, green, yellow and red lines respectively, for the DJFMAM season. A similar plot is shown in Figure 10d for the JJASON season. CATS extinction profiles for the daily average as well averages for the four selected times are similar, suggesting that minor temporal variations in CATS extinctions can be expected for global averages.

Those global averages are dominated by CATS profiles from global oceans (Figure 10b and 10e), which also have small diurnal variations, as ~70% of the globe is covered by water. In comparison, noticeable diurnal changes in aerosol vertical distributions are found over land as shown in Figure 10c and 10f. For the DJFMAM season, at the 1 km altitude, the minimum and maximum aerosol extinctions are at 12 and 18 UTC respectively. Similarly, the minimum and maximum aerosol extinctions are at 12 and 00 UTC at the altitude of 400 m. For the JJASON season, the minimum aerosol extinction values are found at 12 UTC for the whole 0-2 km column, while the maximum aerosol extinction values are at 18UTC for 1.5 km and 00 UTC for the 300-400 m altitude. Still, it should be noted that aerosol concentrations may be a function of local time, yet for a given UTC time, local times will vary by region. Also, due to solar contamination, nighttime retrievals from CATS are significantly and demonstrably less noisy than daytime retrievals, and this difference in sensor sensitivity between day and night may further affect the derived diurnal variations in CATS AOD and aerosol vertical profiles as shown in Figure 3 for individual retrievals. Still, no apparent solar pattern is detectable from Figure 8, and only minor diurnal variations are found for Figure 10a and 10d, which indicate that such a solar contamination may introduce noise but not bias to daytime aerosol retrievals, from a global mean perspective.

If we examine the mean global CATS extinction vertical profiles with respect to local time as shown in Figure 11, however, some distinct features appear. For example, Figure 11a and 11d suggests that on global average, the minimum aerosol extinction below 1 km is found at 6:00 pm local time, for both JJASON and DJFMAM seasons. Similar patterns are also observed for over global oceans. However, for over land cases, for both seasons, the minimum and maximum aerosol extinction below 600 m is found at 12:00 pm and 00:00/06:00 am local time.

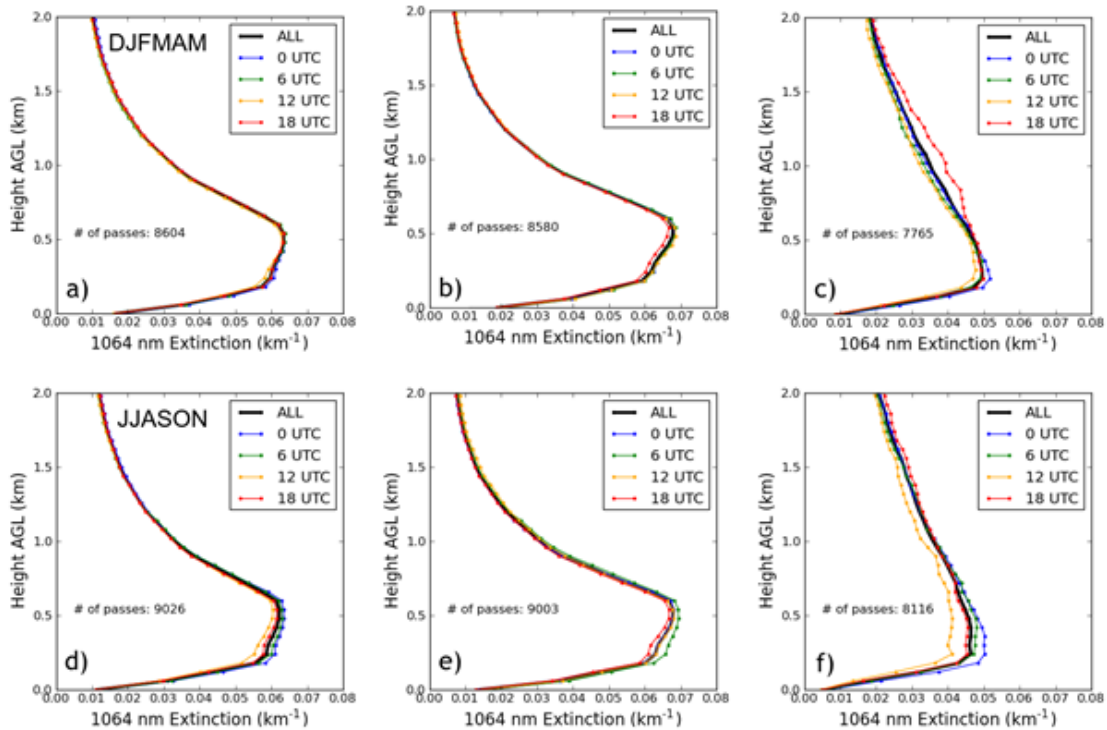


Figure 10: Global mean 6-hourly vertical profiles of CATS 1064 nm extinction for a) DJFMAM all profiles, b) DJFMAM water profiles, c) DJFMAM not-water profiles, d) JJASON all profiles, e) JJASON water profiles, f) JJASON not-water profiles. Mean AODs are as follows: a) 0.084, b) 0.078, c) 0.098, d) 0.089, e) 0.082, and f) 0.102.

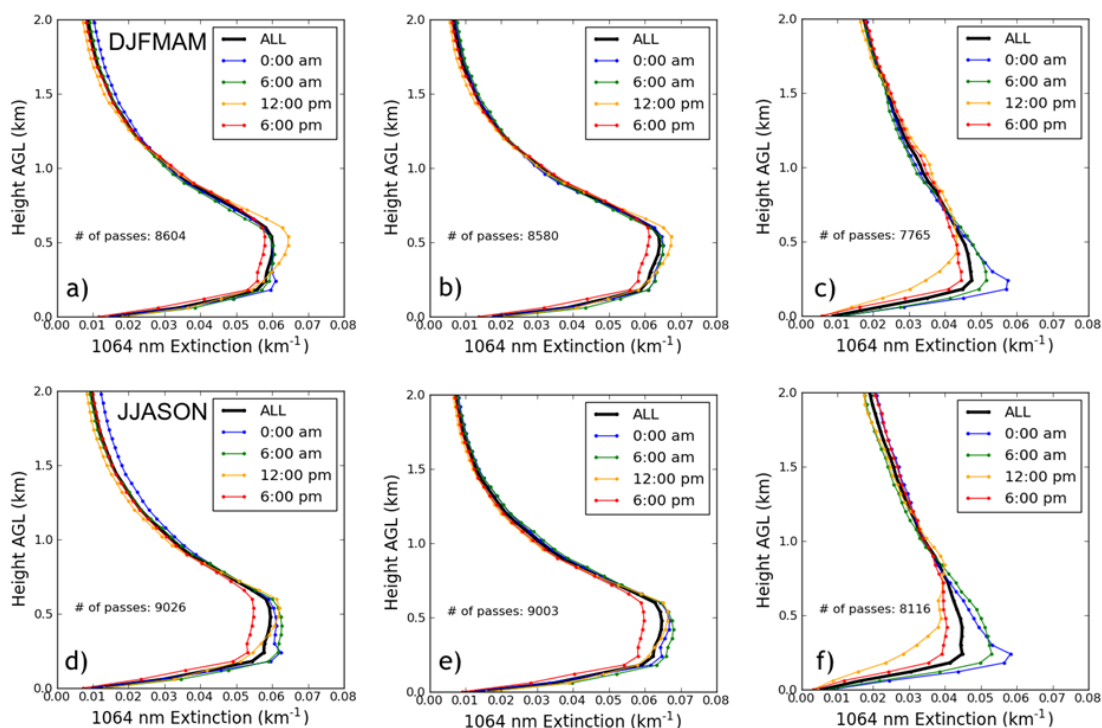


Figure 11: Global mean 6-hourly local time (0:00 am, 6:00 am, 12:00 pm and 6:00 pm) vertical profiles of CATS 1064 nm extinction for a) DJFMAM all profiles, b) DJFMAM water profiles, c) DJFMAM not-water profiles, d) JJASON all profiles, e) JJASON water profiles, f) JJASON not-water profiles. Mean AODs are as follows: a) 0.080, b) 0.079, c) 0.095, d) 0.082, e) 0.081, and f) 0.105.

3.5.3 Diurnal variations of Aerosol Extinction on a Regional Scale (at local time)

In this section, the diurnal variations of aerosol vertical distributions are studied as a function of local solar time for selected regions with high mean AODs as highlighted in Figure 6. Note a near 1 to 1 transformation can be achieved between UTC and local solar time. Also, as learned from the previous section, aerosol features are likely to have a local time dependency. A total of four regions, including Africa-North, Middle East, India and Northeast China, which show significant seasonal mean AODs in Figure 6, are selected for the DJFMAM season (Figure 12). For the JJASON season (Figure 13), in addition to the above mentioned 4 regions, the Africa-South region is also included due to biomass burning in the region during the Northern Hemisphere summer time. The

latitude/longitude boundary of each selected region is described in Table 4. Regional-based analyses are also conducted for 4 selected regions for the DJFMAM season and 5 selected regions for the JJASON season at four local times: 0:00 am (midnight), 6:00 am, 12:00 pm and 6:00 pm, using quality assured CATS profiles. Generally, the maximum diurnal change in aerosol extinction is found at the altitude of below 1 km for all regions as well for both seasons. Also, larger diurnal variations in vertical distributions of aerosol extinction are found for the JJASON season, in-comparing with the DJFMAM season, while regional-based differences are apparent.

For the Africa-North region, dominant aerosol types are dust and smoke aerosol for the DJFMAM season, and dust for the JJASON season (e.g., Remer et al. 2008). Interestingly, the maximum aerosol extinction below 500m is found at 6:00 am for the DJFMAM season. While for the JJASON season, the maximum aerosol extinctions are found at 0:00 am / 6:00 am for the 100-500 m layer, with a significant ~10-20% higher aerosol extinction from the daily mean. Note that 6:00 am in the Africa-North region corresponds to early morning, which has been identified in several studies (Fiedler et al. 2013; Ryder et al. 2015) as the time of day when nocturnal low-level jet breakdown causes large amounts of dust emission in this region. Thus, we suspect that this 6:00 am peak in maximum aerosol extinctions may be the signal resulting from the low-level jet ejection mechanism captured on a regional scale. As the day progresses into the afternoon and early evening, we find the aerosol heights shifting upwards, likely related to the boundary layer's mixed layer development.

For the Middle East region, for the JJASON season, a daily maximum in aerosol extinction of $\sim 0.15 \text{ km}^{-1}$ is found at midnight (0:00 am), with a daily minimum of ~ 0.08

km^{-1} found at local noon (12:00 pm), for the peak aerosol extinction layer that has a daily mean aerosol extinction of $\sim 0.12 \text{ km}^{-1}$. This translates to a $\sim \pm 20\text{-}30\%$ daily variation for aerosol extinction for the peak aerosol extinction layer. Smaller daily variation in aerosol extinction, however, is found for the same region for the DJFMAM season.

For the India region, for the JJASON season, a large peak in aerosol extinction of up to 10% higher than daily mean is found at 6:00 am below 500 m. The minimum aerosol extinction is found at 12:00/6:00 pm for the layer below 500 m, and is overall $\sim 10\%$ lower than the peak daily mean aerosol extinction value. For the DJFMAM season, minimum aerosol extinctions are found at 12:00 pm for near the whole 0-2 km column, while for the layer below 500 m, the maximum aerosol extinction values are found at mid-night (0:00 am).

For the Northeast China region, a significant peak found at the 500 m-1 km layer for local afternoon (6:00 pm) for the DJFMAM season. A similar feature is also found for the JJASON season. While the peak extinction for the JJASON season happens at 06:00am for the aerosol layer below 500m. Lastly, for the Africa-South region, biomass burning aerosols are prevalent during the summer time and thus only the JJASON season is analyzed. As shown in 13b, below 500m in altitude, lower extinction values are found for local afternoon (6:00 pm) and higher extinction values are found for local morning or early morning (0:00 and 6:00 am).

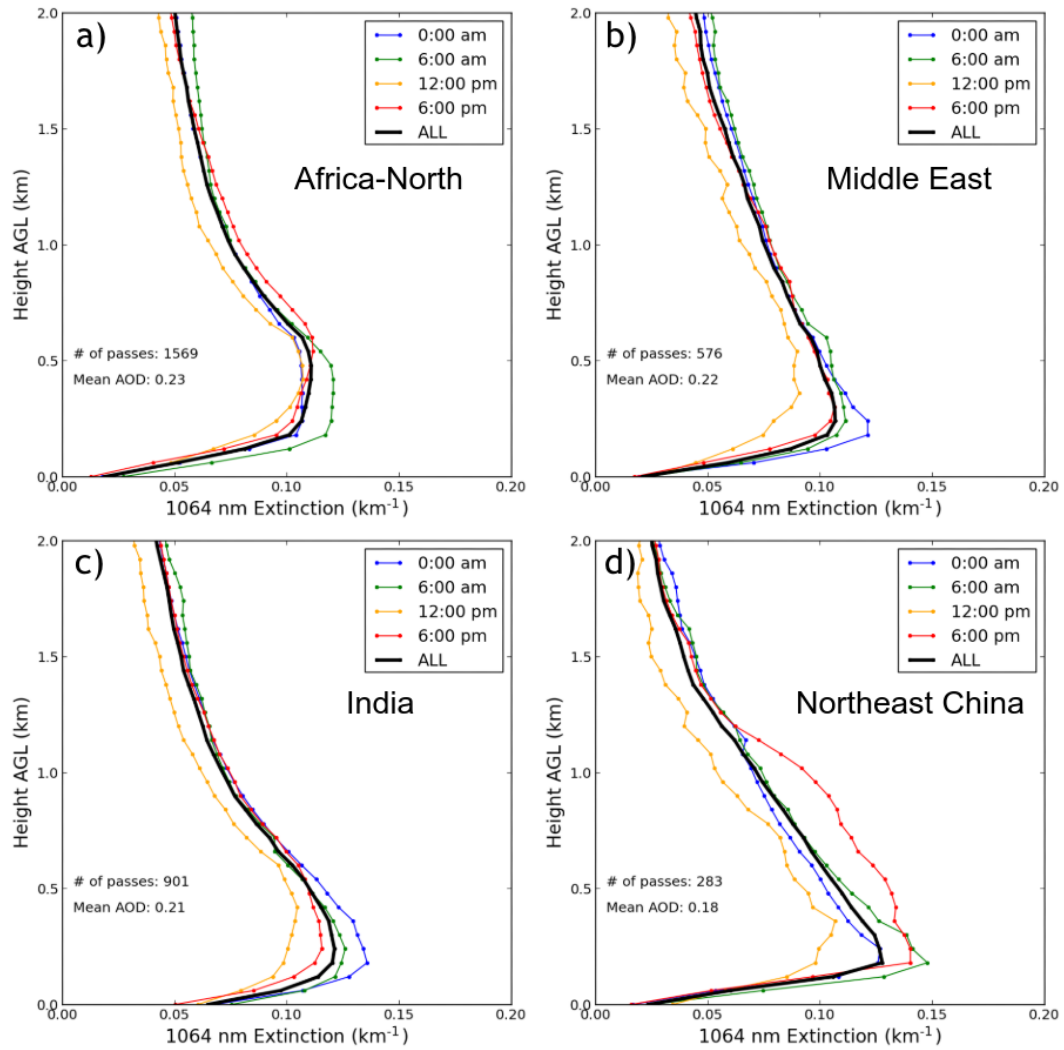


Figure 12: DJFMAM 6-hourly average (local time; 0:00 am, 6:00 am, 12:00 pm and 6:00 pm) vertical profiles of CATS 1064 nm for locations shown in Figure 6a; a) Africa-North, b) Middle East, c) India, and d) Northeast China.

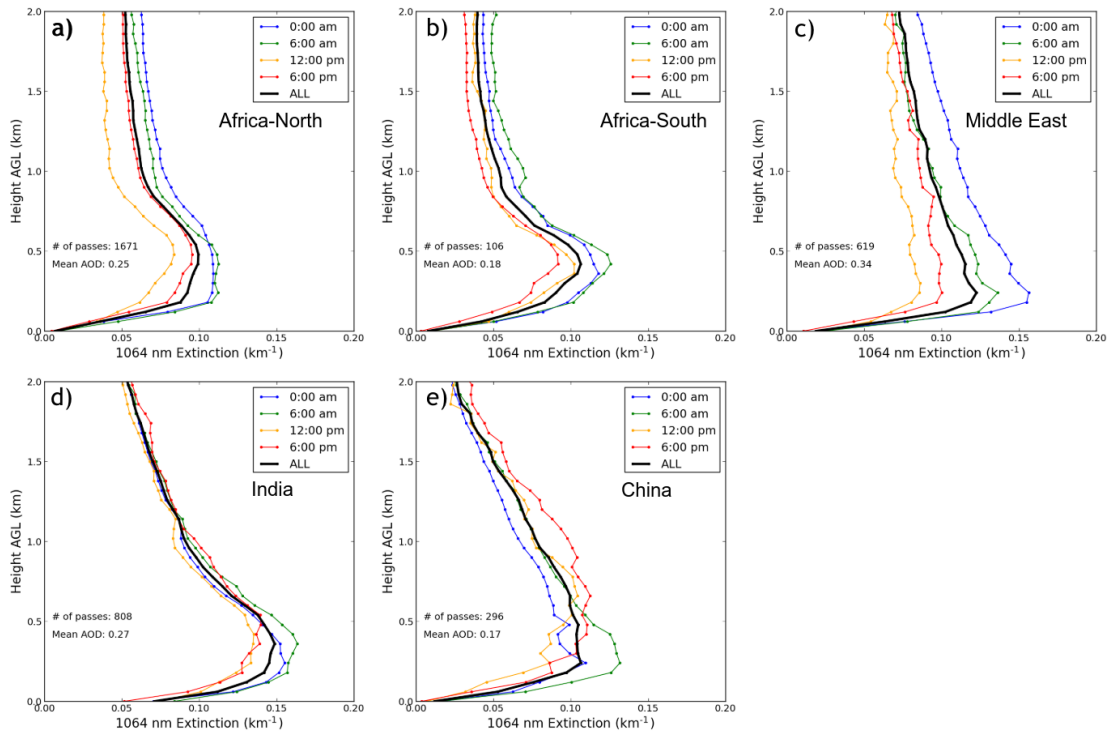


Figure 13: JJASON 6-hourly average (local time; 0:00 am, 6:00 am, 12:00 pm and 6:00 pm) vertical profiles of CATS 1064 nm for locations shown in Figure 6b; a) Africa-North, b) Africa-South, c) Middle East, d) India, and e) Northeast China.

Table 4: Geographic ranges, height above ground level of maximum extinction, diurnal extinction range at height of maximum extinction, and time (local) of peak extinction for the boxed red regions in Figure 6 and vertical profiles shown in Figures 12 and 13.

DJFMAM/JJASON					
Region	Latitude	Longitude	Height AGL (m) of Max. Extinction	Extinction Range (km ⁻¹) at Height AGL of Max. Extinction	Time of Peak Extinction at Height AGL of Max. Extinction
India	7.5°N - 32.5°N	65°E - 85°E	180/360	0.099-0.136/0.135-0.163	0 am/6 am
Africa - North	2.5°N - 22.5°N	35°W - 20°E	420/420	0.107-0.121/0.082-0.113	6 am/6 am
Africa - South	17.5°S - 2.5°N	0° - 30°E	/420	/0.092-0.126	/6 am
Middle East	12.5°N - 27.5°N	35°E - 50°E	180/240	0.075-0.121/0.086-0.156	0 am/0 am
China	27.5°N - 37.5°N	110°E - 120°E	180/240	0.098-0.148/0.086-0.132	6 am/6 am

3.5.4 Comparison to Previous Studies

One of the more notable results of this study is the large diurnal variability in AOD and also in aerosol vertical extinction (with extinction peaks during nighttime-early morning) over regions with high AOD. However, this seems to contradict Smirnov et al. (2002), which studied aerosol diurnal variability during the daytime using AERONET at multiple sites based on 4 dominant aerosol types: urban, dust, biomass burning, and marine aerosols. Overall, that study found an increasing trend in aerosol optical depth during the afternoon for urban aerosol sites and those impacted by local smoke emissions. In addition, Smirnov et al. (2002) found only small diurnal variability at dust-dominated sites (within about 5% of the daily mean) with varying trends among different sites. The reasons for these apparent discrepancies are not immediately clear, but given that AERONET measurements were limited to the daytime in Smirnov et al. (2002) and lidars are more susceptible to daytime noise, a more thorough examination of the impact of this noise on daytime lidar signals and feature detection from CATS might be prudent even though we did not find any apparent daytime bias in this study (e.g. Figure 4). It should also be noted that AERONET sites are inherently point observations with limited locations, which does not provide the same spatial coverage of CATS and may contribute to sampling-related discrepancies.

Interestingly, there were similarities with another lidar-based global study by Huang et al. (2013). In that study, mean CALIOP 532 nm vertical extinction profiles and the difference between daytime and nighttime 532 nm vertical extinction profiles were studied for several regions for four seasons: Dec.-Feb. (DJF), Mar.-May (MAM), Jun.-July (JJA), and Sep.-Nov. (SON). Similar to this CATS study, larger extinction was

generally found during nighttime, which the authors suspected could be due to solar impact on aerosol detection sensitivity during the daytime. Also similar to this CATS study, low-level peaks in extinction were found below 1 km for broadly defined regions encompassing northern Africa (which includes parts of the Africa-North and Middle East regions from this CATS study), southern Africa, India, and eastern China, in all seasons, with a stronger peak in the JJA season for northern Africa. Different from this CATS study, however, was a notable peak in extinction around 3 km for southern Africa in the SON/DJF seasons which the authors attributed to dust in the upper levels. Given the longer 6-month seasonal averages computed in this CATS study (DJFMAM and JJASON), it's possible some of that signal could have been masked by the chosen seasonal classification.

It is also possible that higher nighttime extinction as reported from Huang et al. (2013) and this study may be linked to physical reasons such as higher relative humidity at nighttime, which has been associated with hygroscopic aerosol growth and production of secondary aerosols (Qu et al. 2015). It is interesting to note that higher nighttime/early morning Particulate Matter (PM) concentrations are also reported from several regions using ground-based observations of PM concentrations (e.g. Huang et al., 2015; Dhaka et al., 2020; Dobson et al., 2021). The reported increase in nighttime/early morning surface PM concentration in those studies may plausibly be related to lower planetary boundary (PBL) height, which deserves future study.

3.5.5 Some Potential Mechanisms for Diurnal Aerosol Variability

Given the large diurnal variability in aerosol optical depth and vertical extinction identified in the CATS data over several regions, it is important to examine potential

physical mechanisms which could be responsible for aerosol variability over short time scales in addition to the reasons mentioned in the previous section (e.g. PBL height and RH). Here, 3 documented and distinct mechanisms which can result in diurnal aerosol variability will be discussed: 1) nocturnal low-level jet breakdown, 2) convectively-generated haboobs, and 3) anthropogenic sources.

1) Breakdown of the Nocturnal Low-Level Jet

Low-level jets are jet streams, or narrow streams of relatively strong winds, occurring in the lower part of the troposphere (American Meteorological Society 2020). Nocturnal low-level jets are a subset of low-level jets which occur at night. The formation of these jets has been attributed to several meteorological conditions, such as inertial oscillations, differential heating/baroclinicity in sloping terrain or near land-sea contrasts, orographic channeling, and synoptic baroclinicity associated with weather systems (Fielder et al. 2013; Stull 1988), but a common feature to these mechanisms is development of a stable nocturnal boundary layer which allows winds to “decouple” from the surface, reducing the influence of surface friction. This allows the wind speed above the nocturnal boundary layer to accelerate into a “low-level jet” of air in the lower atmosphere (Lin 2007). With sunrise, the commencement of surface heating helps to re-establish turbulent mixing of the air aloft and near the surface, mixing momentum from the nocturnal low-level jet toward the surface and resulting in dust emission due to the resultant increase in surface wind speeds (Fielder et al. 2013). In studying nocturnal low-level jets in north Africa, Fielder et al. (2013) found a peak in dust emission around 9 AM Local Time, with 15% of north African dust emission annually associated with

nocturnal low-level jet breakdown. This could explain some of the 6:00 am (local time) peaks in extinction for Africa-North and the Middle East in this study.

2) Convectively-Generated Haboobs

Haboobs are intense dust storms caused by strong winds which result in lofted dust and significant reductions in visibility (American Meteorological Society 2020). While larger scale synoptic pressure gradients can generate haboobs, they are also caused by convective (i.e. thunderstorm) outflow (Warner 2009). In the latter case, as rain from thunderstorms falls into a relatively dry environment, it evaporates, with evaporative cooling generating a strong cold pool (or density current) which then spreads out at the surface away from the storm. The advancing cold pool is often characterized by enhanced turbulence and gusty winds, which loft dust from the surface (Roberts and Knippertz 2012).

Notable examples of this phenomenon are found in the Saharan desert. Knippertz et al. (2007) observed several cases of thunderstorm formation over the Atlas Mountains northwest of the Sahara (attributed at least in part to differential heating over sloping terrain) as part of the Saharan Mineral Dust Experiment (SAMUM) field campaign, with density currents forming with mid-day convection, then propagating down-slope into the low-lands of the Sahara by late afternoon and evening and eventually dissipating overnight. Strong acceleration of the wind was observed behind the leading edge of the density current, with reduced visibility/increased dust concentration. Haboobs originating from thunderstorms initiated over the higher terrain of the Aïr and Hoggar mountains within the Sahara were also noted by Roberts and Knippertz (2014).

Another example of haboobs as a dust lofting mechanism is the generation of haboobs during the West-African Monsoon. Moist monsoonal air in the Sahel region south of the Sahara can act as a density current and cause dust emission as it advances northward (Bou Karam et al. 2008), with associated convection producing haboobs propagating into the Sahara and leading to dust transport and emission, even during nighttime hours (Marsham et al. 2008; Cuesta et al. 2020). Haboobs have also been identified as a source of dust emission in the Middle East (Miller et al. 2008). It is possible that some of the 0:00 am (local time) peaks in extinction in this study are related to dust associated with cold pools arriving nocturnally, though once again we might not expect all regions to be prone to nighttime haboobs and thus this likely would not account for all of the 0:00 am peaks.

3) Anthropogenic Sources

Anthropogenic (human-influenced) activity has also been linked to diurnal aerosol variation. Garland et al. (2009) used a photoacoustic spectrometer to study ground-based 532 nm wavelength aerosol particle scattering and absorption coefficients south of Beijing. A notable peak in the absorption coefficient was found during the morning hours, coinciding with an increase in carbon monoxide and nitrogen oxide and suggesting a connection to local combustion. This CATS study also noted peaks in low-level extinction around 6:00 am local time, which could coincide with similar local emission. Garland et al. (2009) also reported higher absorption and scattering coefficients in late evening through early morning than during the afternoon, which the authors attributed to continued local emission into the stable nocturnal boundary layer. In

another study, Alföldy et al. (2007) found high correlation between daily mean sulfur dioxide levels, typically attributed to fuel combustion, and aerosol optical depth in Budapest. Biomass burning in southern Africa has also been linked to diurnal aerosol variability. Although limited to daytime measurements, Eck et al. (2003) used sun-sky radiometers to study aerosol optical depth variability during the daytime in southern Africa. 500 nm AOD was found to increase during the afternoon at several sites in Zambia (an active fire region during the study), which was attributed to an increase in local biomass burning due to the warmer and dryer conditions present in the afternoons. Interestingly, this increasing daytime trend was not apparent in the extinction plots for Africa-South in this CATS study, which once again suggests more thorough examination of daytime data or a more focused study of heavy aerosol-polluted regions like the one mentioned in Eck et al. (2003) is needed.

Chapter 4

Conclusion

Using CALIOP, MODIS and AERONET data, CATS derived AODs as well as vertical distributions of aerosol extinctions were evaluated for the study period of Mar. 2015 – Oct. 2017. CATS data (at 1064 nm) were further used to study variations in AODs and aerosol vertical distributions diurnally. Findings included:

- (1) Quality assurance steps are critical for applying CATS data in aerosol related applications. With a less than 2% data loss due to QA steps, an improvement in correlation from 0.51 to 0.65 is found for the collocated CATS and AERONET AOD comparisons. Using quality assured CATS data, reasonable agreements are found between CATS derived AODs and AODs from CALIOP, Aqua MODIS DT and Terra MODIS DT at the same local times, with correlations of 0.74, 0.74 and 0.72 respectively.
- (2) While the averaged vertical distributions from CATS compare reasonably well with that from CALIOP, differences in peak extinction altitudes are present. This may be due to sampling difference as well as algorithm and instrument differences such as different lidar ratios used.
- (3) From the global mean perspective, minor changes are found for AODs at four selected times, namely 00, 06, 12 and 18 UTC. Yet noticeable diurnal variations in AODs of above 0.10 (at 1064 nm) are found for regions with extensive aerosol events, such as over Africa-North, Middle East, and India for the DJFMAM season, and over Northern and Africa-South, India and Middle East for the JJASON season.

- (4) From the global mean perspective, changes are less noticeable for the averaged aerosol extinction profiles at 00, 06, 12 and 18 UTC. Yet, if the study is repeated with respect to local time, a peak in aerosol extinction is found for local noon (12:00pm) for the DJFMAM season and the minimum value in aerosol extinction is found at 6:00 pm local time for both JJASON and DJFMAM seasons. While the over water aerosol vertical distributions are similar to the global means, for over land cases, the minimum and maximum extinctions are found at local noon (12:00pm) and local morning or early morning (6:00am and 0:00am) for the layer below 500 m for both seasons.
- (5) Larger diurnal variations are found in regions with heavy aerosol plumes such as Northern and Southern (summer season only) Africa, Middle East, India and Eastern China. In particular, aerosol extinctions from 6:00 am over Africa-North are ~10% higher than daily means for the 0-500 m column for both seasons. This may be related to increase in dust concentrations due to breakdown of low level jets at early morning time for the region.
- (6) Still, readers should be aware that AOD retrievals at the 1064 nm are less sensitive to fine mode aerosols such as smoke and pollutant aerosols, compared to coarse mode aerosols such as dust aerosols (e.g., Dubovik et al. 2000). Thus, an investigation of diurnal variations of aerosol properties at the visible channel may be also needed for a future study.

This paper suggests that strong regional diurnal variations exist for both AOD and aerosol extinction profiles. Still, at present these conclusions are tentative, and will remain so until a comprehensive analysis of the CATS calibration accuracy and stability

is completed. These results demonstrate the need for global aerosol measurements throughout the entire diurnal cycle to improve visibility and particulate matter forecasts as well as studies focused on aerosol climate applications. Given the above findings and limitations, a few key ideas are suggested for future work:

- 1) While this study did not find a diurnal bias in CATS data, it is important to closely examine how added solar noise during the day impacts the CATS AOD signal. Comparison between CATS and AERONET AOD as a function of local time on global and regional scales might shed more light on this topic, and also help to solidify patterns of diurnal variability seen in this study (e.g. Figure 8). In addition, this could be expanded to include comparisons to several other global satellite sensors with different observing times in the diurnal cycle, though differences in calibration between the sensors may prove difficult to overcome.
- 2) More quantitative comparisons of CATS and CALIOP vertical extinction profiles should be performed, especially in the context of discovering the source of discrepancies between the two sensors. Case studies of when these sensors overlap but show differences could be particularly illuminating.
- 3) An effort should be made to tie CATS diurnal variability in both AOD and vertical extinction profiles to the meteorological conditions behind them. While several possible sources of diurnal variability were discussed in this study, it is crucial that the processes behind the signals are understood for modeling applications. Utilizing observations, ground-based lidar and photometer networks, and meteorological reanalysis data could be particularly useful in identifying

extinction profiles and AOD distribution based on synoptic and mesoscale weather features.

APPENDIX A:

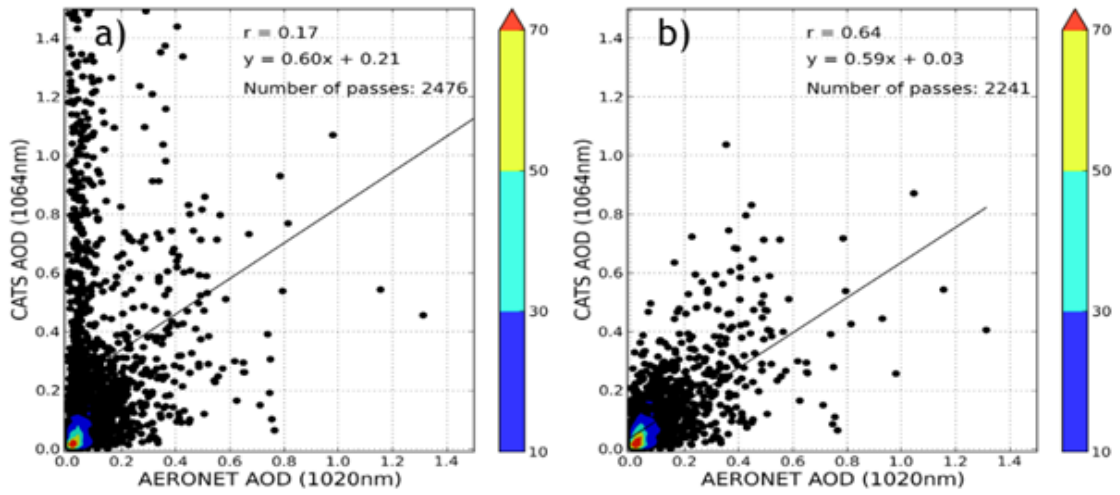


Figure A1: Collocated AERONET 1020 nm AOT vs. CATS 1064 nm AOD a) without CATS QA applied, and b) with CATS QA applied. CATS V2-01 aerosol products were used in constructing this plot.

References

- Aerosol Product Application Team of the AWG Aerosols/Air Quality/Atmospheric Chemistry Team, 2012: GOES-R Advanced Baseline Imager (ABI) algorithm theoretical basis document for suspended matter/aerosol optical depth and aerosol size parameter. NOAA/NESDIS/STAR, Accessed 4 October 2021, <https://www.star.nesdis.noaa.gov/goesr/docs/ATBD/AOD.pdf>.
- Alfaro-Contreras, R., J. Zhang, J. R. Campbell, and J. S. Reid, 2016: Investigating the frequency and interannual variability in global above-cloud aerosol characteristics with CALIOP and OMI. *Atmospheric Chemistry and Physics*, **16**, 47–69, <https://doi.org/10.5194/acp-16-47-2016>.
- Alföldy, B., J. Osán, Z. Tóth, S. Török, A. Harbusch, C. Jahn, S. Emeis, and K. Schäfer, 2007: Aerosol optical depth, aerosol composition and air pollution during summer and winter conditions in Budapest. *Science of The Total Environment*, **383**, 141–163, <https://doi.org/10.1016/j.scitotenv.2007.04.037>.
- American Meteorological Society, 2020: Glossary of Meteorology. Accessed 10 November 2021, <https://glossary.ametsoc.org/wiki/https://glossary.ametsoc.org/wiki/>.
- Bou Karam, D., C. Flamant, P. Knippertz, O. Reitebuch, J. Pelon, M. Chong, and A. Dabas, 2008: Dust emissions over the Sahel associated with the West African monsoon intertropical discontinuity region: A representative case-study. *Quarterly Journal of the Royal Meteorological Society*, **134**, 621–634, <https://doi.org/10.1002/qj.244>.

Campbell, J. R., and Coauthors, 2012: Evaluating nighttime CALIOP 0.532 μm aerosol optical depth and extinction coefficient retrievals. *Atmospheric measurement techniques*, **5**, 2143–2160, <https://doi.org/10.5194/amt-5-2143-2012>.

Carson-Marquis, B. N., J. Zhang, P. Xian, J. S. Reid, and J. W. Marquis, 2021: Improving WRF-Chem Meteorological Analyses and Forecasts over Aerosol-Polluted Regions by Incorporating NAAPS Aerosol Analyses. *Journal of Applied Meteorology and Climatology*, **60**, 839–855, <https://doi.org/10.1175/JAMC-D-20-0174.1>.

Cuesta, J., and Coauthors, 2020: Three-dimensional pathways of dust over the Sahara during summer 2011 as revealed by new Infrared Atmospheric Sounding Interferometer observations. *Quarterly Journal of the Royal Meteorological Society*, **146**, 2731–2755, <https://doi.org/10.1002/qj.3814>.

Dhaka, S.K., Chetna, Kumar, V. *et al.* PM_{2.5} diminution and haze events over Delhi during the COVID-19 lockdown period: an interplay between the baseline pollution and meteorology. *Sci Rep* **10**, 13442 (2020). <https://doi.org/10.1038/s41598-020-70179-8>.

Dobson R, Siddiqi K, Ferdous T, et al. Diurnal variability of fine-particulate pollution concentrations: data from 14 low- and middle-income countries. *Int J Tuberc Lung Dis*. 2021;25(3):206-214. doi:10.5588/ijtld.20.0704.

Dubovik, O., A. Smirnov, B. N. Holben, M. D. King, Y. J. Kaufman, T. F. Eck, and I. Slutsker, 2000: Accuracy assessments of aerosol optical properties retrieved from Aerosol Robotic Network (AERONET) Sun and sky radiance measurements. *Journal of Geophysical Research: Atmospheres*, **105**, 9791–9806, <https://doi.org/10.1029/2000JD900040>.

Eck, T. F., and Coauthors, 2003: Variability of biomass burning aerosol optical characteristics in southern Africa during the SAFARI 2000 dry season campaign and a comparison of single scattering albedo estimates from radiometric measurements.

Journal of Geophysical Research: Atmospheres, **108**,

<https://doi.org/10.1029/2002JD002321>.

Eck, T. F., and Coauthors, 2013: A seasonal trend of single scattering albedo in southern African biomass-burning particles: Implications for satellite products and estimates of emissions for the world's largest biomass-burning source. *Journal of Geophysical*

Research: Atmospheres, **118**, 6414–6432, <https://doi.org/10.1002/jgrd.50500>.

Fiedler, S., K. Schepanski, B. Heinold, P. Knippertz, and I. Tegen, 2013: Climatology of nocturnal low-level jets over North Africa and implications for modeling mineral dust emission. *Journal of Geophysical Research: Atmospheres*, **118**, 6100–6121,

<https://doi.org/10.1002/jgrd.50394>.

Garland, R. M., and Coauthors, 2009: Aerosol optical properties observed during Campaign of Air Quality Research in Beijing 2006 (CAREBeijing-2006): Characteristic differences between the inflow and outflow of Beijing city air. *Journal of Geophysical*

Research: Atmospheres, **114**, <https://doi.org/10.1029/2008JD010780>.

Giglio, L., J. D. Kendall, and R. Mack, 2003: A multi-year active fire dataset for the tropics derived from the TRMM VIRS. *International Journal of Remote Sensing*, **24**, 4505–4525, <https://doi.org/10.1080/0143116031000070283>.

Giles, D. M., and Coauthors, 2019: Advancements in the Aerosol Robotic Network (AERONET) Version 3 database – automated near-real-time quality control algorithm

with improved cloud screening for Sun photometer aerosol optical depth (AOD) measurements. *Atmospheric Measurement Techniques*, **12**, 169–209, <https://doi.org/10.5194/amt-12-169-2019>.

Hartmann, D. L., 2016: *Global Physical Climatology*. Elsevier Science, 498 pp.

Heinold, B., P. Knippertz, J. H. Marsham, S. Fiedler, N. S. Dixon, K. Schepanski, B. Laurent, and I. Tegen, 2013: The role of deep convection and nocturnal low-level jets for dust emission in summertime West Africa: Estimates from convection-permitting simulations. *Journal of Geophysical Research: Atmospheres*, **118**, 4385–4400, <https://doi.org/10.1002/jgrd.50402>.

Holben, B. N., and Coauthors, 1998: AERONET—A Federated Instrument Network and Data Archive for Aerosol Characterization. *Remote Sensing of Environment*, **66**, 1–16, [https://doi.org/10.1016/S0034-4257\(98\)00031-5](https://doi.org/10.1016/S0034-4257(98)00031-5).

Huang, L., J. H. Jiang, J. L. Tackett, H. Su, and R. Fu, 2013: Seasonal and diurnal variations of aerosol extinction profile and type distribution from CALIPSO 5-year observations. *Journal of Geophysical Research: Atmospheres*, **118**, 4572–4596, <https://doi.org/10.1002/jgrd.50407>.

Huang F, Li X, Wang C, Xu Q, Wang W, Luo Y, et al. (2015) PM_{2.5} Spatiotemporal Variations and the Relationship with Meteorological Factors during 2013-2014 in Beijing, China. *PLoS ONE* 10(11): e0141642. <https://doi.org/10.1371/journal.pone.0141642>

Hyer, E. J., J. S. Reid, E. M. Prins, J. P. Hoffman, C. C. Schmidt, J. I. Miettinen, and L. Giglio, 2013: Patterns of fire activity over Indonesia and Malaysia from polar and

geostationary satellite observations. *Atmospheric Research*, **122**, 504–519, <https://doi.org/10.1016/j.atmosres.2012.06.011>.

Kaku, K. C., J. S. Reid, J. L. Hand, E. S. Edgerton, B. N. Holben, J. Zhang, and R. E. Holz, 2018: Assessing the Challenges of Surface-Level Aerosol Mass Estimates From Remote Sensing During the SEAC4RS and SEARCH Campaigns: Baseline Surface Observations and Remote Sensing in the Southeastern United States. *Journal of Geophysical Research: Atmospheres*, **123**, 7530–7562, <https://doi.org/10.1029/2017JD028074>.

Kaufman, Y. J., D. Tanré, and O. Boucher, 2002: A satellite view of aerosols in the climate system. *Nature*, **419**, 215–223, <https://doi.org/10.1038/nature01091>.

Knippertz, P., C. Deutscher, K. Kandler, T. Müller, O. Schulz, and L. Schütz, 2007: Dust mobilization due to density currents in the Atlas region: Observations from the Saharan Mineral Dust Experiment 2006 field campaign. *Journal of Geophysical Research: Atmospheres*, **112**, <https://doi.org/10.1029/2007JD008774>.

Levy, R. C., S. Mattoo, L. A. Munchak, L. A. Remer, A. M. Sayer, F. Patadia, and N. C. Hsu, 2013: The Collection 6 MODIS aerosol products over land and ocean. *Atmospheric Measurement Techniques*, **6**, 2989–3034, <https://doi.org/10.5194/amt-6-2989-2013>.

Lin, Y.-L., 2007: *Mesoscale Dynamics*. Cambridge University Press, 630 pp.

Liu, Z., and Coauthors, 2009: The CALIPSO Lidar Cloud and Aerosol Discrimination: Version 2 Algorithm and Initial Assessment of Performance. *Journal of Atmospheric and Oceanic Technology*, **26**, 1198–1213, <https://doi.org/10.1175/2009JTECHA1229.1>.

- Lynch, P., and Coauthors, 2016: An 11-year global gridded aerosol optical thickness reanalysis (v1.0) for atmospheric and climate sciences. *Geoscientific Model Development*, **9**, 1489–1522, <https://doi.org/10.5194/gmd-9-1489-2016>.
- Marsham, J. H., D. J. Parker, C. M. Grams, C. M. Taylor, and J. M. Haywood, 2008: Uplift of Saharan dust south of the intertropical discontinuity. *Journal of Geophysical Research: Atmospheres*, **113**, <https://doi.org/10.1029/2008JD009844>.
- Mbourou, G. N., J. J. Bertrand, and S. E. Nicholson, 1997: The Diurnal and Seasonal Cycles of Wind-Borne Dust over Africa North of the Equator. *Journal of Applied Meteorology and Climatology*, **36**, 868–882, [https://doi.org/10.1175/1520-0450\(1997\)036<0868:TDASCO>2.0.CO;2](https://doi.org/10.1175/1520-0450(1997)036<0868:TDASCO>2.0.CO;2).
- McGill, M. J., J. E. Yorks, V. S. Scott, A. W. Kupchok, and P. A. Selmer, 2015: The Cloud-Aerosol Transport System (CATS): a technology demonstration on the International Space Station. *Lidar Remote Sensing for Environmental Monitoring XV*, Vol. 9612 of, *Lidar Remote Sensing for Environmental Monitoring XV*, SPIE, 34–39.
- Miller, S. D., A. P. Kuciauskas, M. Liu, Q. Ji, J. S. Reid, D. W. Breed, A. L. Walker, and A. A. Mandoos, 2008: Haboob dust storms of the southern Arabian Peninsula. *Journal of Geophysical Research: Atmospheres*, **113**, <https://doi.org/10.1029/2007JD008550>.
- NASA CATS Group, 2018: CATS Data Release Notes: L1B Version 3.00, L2O Version 3.00. Accessed 4 October 2021, https://cats.gsfc.nasa.gov/media/docs/CATS_Release_Notes7.pdf.
- Noel, V., H. Chepfer, M. Chiriaco, and J. Yorks, 2018: The diurnal cycle of cloud profiles over land and ocean between 51°S and 51°N, seen by the CATS spaceborne lidar

from the International Space Station. *Atmospheric Chemistry and Physics*, **18**, 9457–9473, <https://doi.org/10.5194/acp-18-9457-2018>.

Omar, A. H., and Coauthors, 2013: CALIOP and AERONET aerosol optical depth comparisons: One size fits none. *Journal of Geophysical Research: Atmospheres*, **118**, 4748–4766, <https://doi.org/10.1002/jgrd.50330>.

Pauly, R. M., and Coauthors, 2019: Cloud-Aerosol Transport System (CATS) 1064 nm calibration and validation. *Atmospheric Measurement Techniques*, **12**, 6241–6258, <https://doi.org/10.5194/amt-12-6241-2019>.

Qu, W. J., J. Wang, X. Y. Zhang, D. Wang, and L. F. Sheng, 2015: Influence of relative humidity on aerosol composition: Impacts on light extinction and visibility impairment at two sites in coastal area of China. *Atmospheric Research*, **153**, 500–511, <https://doi.org/10.1016/j.atmosres.2014.10.009>.

Rajapakshe, C., Z. Zhang, J. E. Yorks, H. Yu, Q. Tan, K. Meyer, S. Platnick, and D. M. Winker, 2017: Seasonally transported aerosol layers over southeast Atlantic are closer to underlying clouds than previously reported. *Geophysical Research Letters*, **44**, 5818–5825, <https://doi.org/10.1002/2017GL073559>.

Ramanathan, V., P. J. Crutzen, J. T. Kiehl, and D. Rosenfeld, 2001: Aerosols, Climate, and the Hydrological Cycle. *Science*, **294**, 2119–2124, <https://doi.org/10.1126/science.1064034>.

Redemann, J., M. A. Vaughan, Q. Zhang, Y. Shinozuka, P. B. Russell, J. M. Livingston, M. Kacenelenbogen, and L. A. Remer, 2012: The comparison of MODIS-Aqua (C5) and

- CALIOP (V2 & V3) aerosol optical depth. *Atmospheric Chemistry and Physics*, **12**, 3025–3043, <https://doi.org/10.5194/acp-12-3025-2012>.
- Reid, J. S., T. F. Eck, S. A. Christopher, P. V. Hobbs, and B. Holben, 1999: Use of the Ångström exponent to estimate the variability of optical and physical properties of aging smoke particles in Brazil. *Journal of Geophysical Research: Atmospheres*, **104**, 27473–27489, <https://doi.org/10.1029/1999JD900833>.
- Remer, L. A., and Coauthors, 2005: The MODIS Aerosol Algorithm, Products, and Validation. *Journal of the Atmospheric Sciences*, **62**, 947–973, <https://doi.org/10.1175/JAS3385.1>.
- Remer, L. A., and Coauthors, 2008: Global aerosol climatology from the MODIS satellite sensors. *Journal of Geophysical Research: Atmospheres*, **113**, <https://doi.org/10.1029/2007JD009661>.
- Roberts, A. J., and P. Knippertz, 2012: Haboobs: convectively generated dust storms in West Africa. *Weather*, **67**, 311–316, <https://doi.org/10.1002/wea.1968>.
- Roberts, A. J., and P. Knippertz, 2014: The formation of a large summertime Saharan dust plume: Convective and synoptic-scale analysis. *Journal of Geophysical Research: Atmospheres*, **119**, 1766–1785, <https://doi.org/10.1002/2013JD020667>.
- Ryder, C. L., and Coauthors, 2015: Advances in understanding mineral dust and boundary layer processes over the Sahara from Fennec aircraft observations. *Atmospheric Chemistry and Physics*, **15**, 8479–8520, <https://doi.org/10.5194/acp-15-8479-2015>.

Shi, Y., J. Zhang, J. S. Reid, E. J. Hyer, T. F. Eck, B. N. Holben, and R. A. Kahn, 2011: A critical examination of spatial biases between MODIS and MISR aerosol products – application for potential AERONET deployment. *Atmospheric Measurement Techniques*, **4**, 2823–2836, <https://doi.org/10.5194/amt-4-2823-2011>.

Shi, Y., J. Zhang, J. S. Reid, E. J. Hyer, and N. C. Hsu, 2013: Critical evaluation of the MODIS Deep Blue aerosol optical depth product for data assimilation over North Africa. *Atmospheric measurement techniques*, **6**, 949–969, <https://doi.org/10.5194/amt-6-949-2013>.

Smirnov, A., B. N. Holben, T. F. Eck, I. Slutsker, B. Chatenet, and R. T. Pinker, 2002: Diurnal variability of aerosol optical depth observed at AERONET (Aerosol Robotic Network) sites. *Geophysical Research Letters*, **29**, 30-1-30–34, <https://doi.org/10.1029/2002GL016305>.

Stephens, G. L., and Coauthors, 2002: THE CLOUDSAT MISSION AND THE A-TRAIN: A New Dimension of Space-Based Observations of Clouds and Precipitation. *Bulletin of the American Meteorological Society*, **83**, 1771–1790, <https://doi.org/10.1175/BAMS-83-12-1771>.

Stull, R. B., 1988: *An introduction to boundary layer meteorology*. Kluwer Academic Publishers, 666 pp.

Tackett, J. L., D. M. Winker, B. J. Getzewich, M. A. Vaughan, S. A. Young, and J. Kar, 2018: CALIPSO lidar level 3 aerosol profile product: version 3 algorithm design. *Atmospheric Measurement Techniques*, **11**, 4129–4152, <https://doi.org/10.5194/amt-11-4129-2018>.

- Tedesco, M., 2015: *Remote Sensing of the Cryosphere*. John Wiley & Sons, 429 pp.
- Tiwari, S., A. K. Srivastava, D. S. Bisht, P. Parmita, M. K. Srivastava, and S. D. Attri, 2013: Diurnal and seasonal variations of black carbon and PM_{2.5} over New Delhi, India: Influence of meteorology. *Atmospheric Research*, **125–126**, 50–62, <https://doi.org/10.1016/j.atmosres.2013.01.011>.
- Toth, T. D., J. Zhang, J. R. Campbell, J. S. Reid, and M. A. Vaughan, 2016: Temporal variability of aerosol optical thickness vertical distribution observed from CALIOP. *Journal of Geophysical Research: Atmospheres*, **121**, 9117–9139, <https://doi.org/10.1002/2015JD024668>.
- Toth, T. D., J. R. Campbell, J. S. Reid, J. L. Tackett, M. A. Vaughan, J. Zhang, and J. W. Marquis, 2018: Minimum aerosol layer detection sensitivities and their subsequent impacts on aerosol optical thickness retrievals in CALIPSO level 2 data products. *Atmospheric Measurement Techniques*, **11**, 499–514, <https://doi.org/10.5194/amt-11-499-2018>.
- Vaughan, M., and Coauthors, 2019: CALIPSO lidar calibration at 1064 nm: version 4 algorithm. *Atmospheric Measurement Techniques*, **12**, 51–82, <https://doi.org/10.5194/amt-12-51-2019>.
- Wallace, J. M., and P. V. Hobbs, 2006: *Atmospheric Science: An Introductory Survey*. Elsevier, 505 pp.
- Warner, T. T., 2009: *Desert Meteorology*. Cambridge University Press, 623 pp.

Weitkamp, C., 2006: *Lidar: Range-Resolved Optical Remote Sensing of the Atmosphere*. Springer Science & Business, 467 pp.

Winker, D. M., M. A. Vaughan, A. Omar, Y. Hu, K. A. Powell, Z. Liu, W. H. Hunt, and S. A. Young, 2009: Overview of the CALIPSO Mission and CALIOP Data Processing Algorithms. *Journal of Atmospheric and Oceanic Technology*, **26**, 2310–2323, <https://doi.org/10.1175/2009JTECHA1281.1>.

Yorks, J. E., S. P. Palm, M. J. McGill, D. L. Hlavka, W. D. Hart, P. A. Selmer, and E. Nowottnick, 2015: CATS Algorithm Theoretical Basis Document. Accessed 4 October, 2021, https://cats.gsfc.nasa.gov/media/docs/CATS_ATBD_V1-02.pdf.

Yorks, J. E., and Coauthors, 2016: An overview of the CATS level 1 processing algorithms and data products. *Geophysical Research Letters*, **43**, 4632–4639, <https://doi.org/10.1002/2016GL068006>.

Yoshida, M., M. Kikuchi, T. M. Nagao, H. Murakami, T. Nomaki, and A. Higurashi, 2018: Common Retrieval of Aerosol Properties for Imaging Satellite Sensors. *Journal of the Meteorological Society of Japan. Ser. II*, **96B**, 193–209, <https://doi.org/10.2151/jmsj.2018-039>.

Young, S. A., M. A. Vaughan, R. E. Kuehn, and D. M. Winker, 2013: The Retrieval of Profiles of Particulate Extinction from Cloud–Aerosol Lidar and Infrared Pathfinder Satellite Observations (CALIPSO) Data: Uncertainty and Error Sensitivity Analyses. *Journal of Atmospheric and Oceanic Technology*, **30**, 395–428, <https://doi.org/10.1175/JTECH-D-12-00046.1>.

Zhang, J., J. S. Reid, M. Christensen, and A. Benedetti, 2016: An evaluation of the impact of aerosol particles on weather forecasts from a biomass burning aerosol event over the Midwestern United States: observational-based analysis of surface temperature. *Atmospheric Chemistry and Physics*, **16**, 6475–6494, <https://doi.org/10.5194/acp-16-6475-2016>.

Zhao, X., X. Zhang, X. Xu, J. Xu, W. Meng, and W. Pu, 2009: Seasonal and diurnal variations of ambient PM_{2.5} concentration in urban and rural environments in Beijing. *Atmospheric Environment*, **43**, 2893–2900, <https://doi.org/10.1016/j.atmosenv.2009.03.009>.